Chapter 19

Development of Sand Spits and Cuspate Forelands with Rhythmic Shapes and Their Deformation by Effects of Construction of Coastal Structures

Takaaki Uda, Masumi Serizawa and Shiho Miyahara

Additional information is available at the end of the chapter

http://dx.doi.org/10.5772/57043

1. Introduction

Zenkovich showed that multiple sand spits with rhythmic shapes may develop in a shallow water body such as the Azov Sea and a lagoon facing Chukchi Sea, as shown in Fig. 1, and called them as the spits of Azov type [1]. Zenkovich concluded that under oblique wave incidence with the angle between the direction normal to the shoreline and the wave direction being larger than 45°, shoreline instability may develop, and during the development of sand spits, the wave-sheltering effect due to the sand spits themselves plays an important role. Ashton et al. [2] adopted this mechanism in their model and successfully modeled this shoreline instability using the upwind scheme in their finite difference method to prevent the numerical instability on the basis of the conventional longshore sand transport formula. Furthermore, this mechanism was called high-angle wave instability in [3]. Littlewood et al. [4] predicted the shoreline of log-spiral bays using their model. Serizawa et al. [5] predicted the development of sand spits and cuspate forelands under oblique wave incidence with the angle between the direction normal to the shoreline and the wave direction being larger than 45°, given a small perturbation in the initial topography, and showed that the three-dimensional (3-D) beach changes of sand spits and cuspate forelands with rhythmic shapes can be predicted using the BG model (a 3-D model for predicting beach changes based on Bagnold's concept). Falqués et al. [6] also predicted the development of sand waves caused by high-angle wave instability using equations similar to that of our model, but not the development of sand spits and cuspate forelands protruding offshore. The sand transport equation of the BG model was derived by applying the concept of the equilibrium slope in [7] and the energetics approach of Bagnold [8]. In the fundamental equation of the BG model in [9], the sand transport flux was assumed to be proportional to the wave energy dissipation rate instead of the third power

of the amplitude of the bottom oscillatory velocity due to waves, and the wave energy dissipation rate was given by that due to wave breaking at each point determined in the calculation of the wave field. Here, the development of sand spits and cuspate forelands with rhythmic shapes were predicted first using this numerical model, and then the effects of the construction of a groin and a breakwater on the development of sand spits and cuspate forelands with rhythmic shapes were investigated using the same model [5, 10].

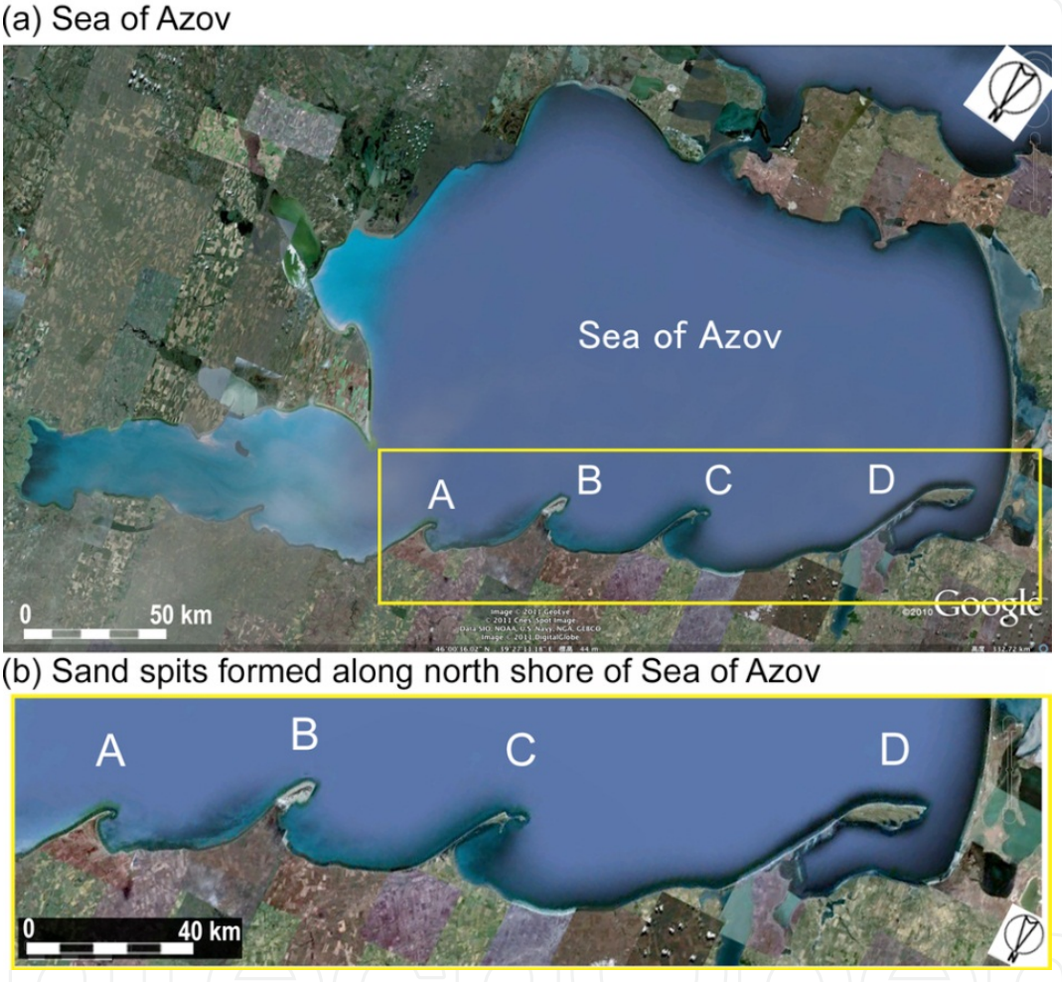

Figure 1. Multiple sand spits with rhythmic shapes developed in Azov-type shallow water body facing Chukchi Sea in Russia [1].

2. Numerical model

We use Cartesian coordinates (x, y) and consider that the elevation at a point Z (x, y, t) is a variable to be solved, where t is the time. The beach changes are assumed to occur between the depth of closure h_c and the berm height h_R. The BG model [9] was used to predict the beach changes. An additional term given by Ozasa and Brampton [11] was incorporated into the fundamental equation of sand transport in the BG model to evaluate the longshore sand

http://dx.doi.org/10.5772/57043

transport due to the effect of the longshore gradient of wave height. The fundamental equation of sand transport is given as follows.

$$\vec{q} = C_0 \frac{P}{\tan\beta_c} \left\{ \begin{array}{l} K_n \left(\tan\beta_c \vec{e_w} - |\cos\alpha| \ \vec{\nabla Z} \right) \\ + \left\{ \left(K_s - K_n \right) \sin\alpha - \dfrac{K_2}{\tan\bar{\beta}} \dfrac{\partial H}{\partial s} \right\} \tan\beta \ \vec{e_s} \end{array} \right\} \quad \left(-h_c \le Z \le h_R \right) \tag{1}$$

Here, $\vec{q}=(q_x, q_y)$ is the net sand transport flux, Z (x, y, t) is the elevation, n and s are the local coordinates taken along the directions normal (shoreward) and parallel to the contour lines, respectively, $\vec{\nabla Z}=(\partial Z/\partial x, \ \partial Z/\partial y)$ is the slope vector, $\vec{e_w}$ is the unit vector of the wave direction, $\vec{e_s}$ is the unit vector parallel to the contour lines, α is the angle between the wave direction and the direction normal to the contour lines, $tan\beta = |\vec{\nabla Z}|$ is the seabed slope, $\tan\beta_c$ is the equilibrium slope, and $tan\beta \ \vec{e_s}=(-\partial Z/\partial y, \ \partial Z/\partial x)$. Moreover, K_s and K_n are the coefficients of longshore and cross-shore sand transport, respectively, K_2 is the coefficient of the Ozasa and Brampton term [11], $\partial H/\partial s = \vec{e_s} \cdot \vec{\nabla H}$ is the longshore gradient of the wave height H measured parallel to the contour lines, and $tan\bar{\beta}$ is the characteristic slope of the breaker zone. In addition, C_0 is the coefficient transforming the immersed weight expression into a volumetric expression ($C_0 = 1/\{(\rho_s - \rho)g(1-p)\}$, where ρ is the density of seawater, ρ_s is the specific gravity of sand particles, p is the porosity of sand and g is the acceleration due to gravity), h_c is the depth of closure, and h_R is the berm height.

The intensity of sand transport P in Eq. (1) is assumed to be proportional to the wave energy dissipation rate [9], on the basis of the energetics approach of Bagnold [8]. P is given by the wave energy dissipation rate due to wave breaking at a local point Φ_{all} (Eq. (2)) in accordance with the BG model in [12], in which the intensity of sand transport is proportional to the wave energy at the breaking point, instead of the assumption that it is proportional to the third power of the amplitude of the bottom oscillatory velocity u_m due to waves.

$$P = \Phi_{all} \tag{2}$$

For the calculation of the wave field, the numerical simulation method using the energy balance equation [13], in which the directional spectrum of irregular waves is the variable to be solved, was employed with an additional term of energy dissipation due to wave breaking [14], similarly to that in [9]. Φ_{all} in Eq. (2) was calculated from Eq. (3), which defines the total sum of the energy dissipation of each component wave due to breaking.

$$\Phi_{all} = f_D E = K\sqrt{g/h}\left[1 - \left(\Gamma/\gamma \right)^2 \right] E \qquad \left(f_D \ge 0 \right) \tag{3}$$

Here, f_D is the energy dissipation rate, E is the wave energy, K is a coefficient expressing the intensity of wave dissipation due to breaking, h is the water depth, Γ is the ratio of the critical wave height to the water depth on a flat bottom, and γ is the ratio of wave height to the water depth H/h. In addition, a lower limit was set for the water depth h in Eq. (3) similarly in [9].

In this method, the energy dissipation rate obtained from the calculation of the plane wave field including the effect of wave dissipation due to breaking was used for the calculation of sand transport. The same approach was employed in [15]. In the calculation of the wave field in the wave run-up zone, an imaginary depth was assumed as in [9]. Furthermore, the wave energy at locations with elevations higher than the berm height was set to 0.

In the numerical simulation of beach changes, the sand transport and continuity equations ($\partial Z / \partial t + \nabla \bullet \vec{q} = 0$) were solved on the x-y plane by the explicit finite-difference method using the staggered mesh scheme. In estimating the intensity of sand transport near the berm top and at the depth of closure, the intensity of sand transport was linearly reduced to 0 near the berm height or the depth of closure to prevent sand from being deposited in the zone higher than the berm height and the beach from being eroded in the zone deeper than the depth of closure, similar to that in [16].

Wave conditions	Incident waves: H_i = 1 m, T = 4 s, wave direction θ_i = 60° relative to direction normal to initial shoreline
Berm height	h_R = 1 m
Depth of closure	h_c = 4 m (still water depth)
Equilibrium slope	$\tan\beta_c$ = 1/20
Angle of repose slope	$\tan\beta_g$ = 1/2
Coefficients of sand transport	Coefficient of longshore sand transport K_s = 0.2 Coefficient of Ozasa and Brampton term [11] K_2 = 1.62K_s Coefficient of cross-shore sand transport K_n = K_s
Mesh size	$\Delta x = \Delta y$ = 20 m
Time intervals	Δt = 0.5 h
Duration of calculation	2.75×10^4 h (5.5×10^4 steps)
Boundary conditions	Shoreward and landward ends: q_x = 0, right and left boundaries: periodic boundary
Calculation of wave field	Energy balance equation [13] •Term of wave dissipation due to wave breaking: Dally et al. model [14] •Wave spectrum of incident waves: directional wave spectrum density in [17] •Total number of frequency components N_F = 1 and number of directional subdivisions N_θ = 8 •Directional spreading parameter S_{max} =25 •Coefficient of wave breaking K = 0.17 and Γ = 0.3 •Imaginary depth between depth h_0 (0.5 m) and berm height h_R •Wave energy = 0 where $Z \geq h/R$ •Lower limit of h in terms of wave decay due to wave breaking: 0.5 m

Table 1. Calculation conditions.

http://dx.doi.org/10.5772/57043

3. Formation of sand spits and cuspate forelands with rhythmic shapes

3.1. Calculation conditions

Ashton and Murray [3] showed that the generation of shoreline instability closely depends on the probability of occurrence of wave directions; sand spits develop in case that the probability of occurrence of a unidirectional waves is high, cuspate bumps develop in case that the probability of occurrence of waves incident from two directions is equivalent, and sand spits with hooked shoreline develop in case that waves are incident from two directions with different probabilities. The calculation conditions in this study were determined referring their results.

For the wave conditions, we assumed H_i = 1 m and T = 4 s, considering the formation of sand spits in a shallow lagoon. The wave direction was assumed to be obliquely incident from 60°, 50° and 40° counterclockwise or from the directions of ±60° with probabilities of 0.5:0.5 and 0.60:0.40, 0.65:0.35, 0.70:0.30, 0.75:0.25 and 0.80:0.20, while determining the direction from the probability distribution at each step. We considered a shallow lake with a flat solid bed, the depth of which was given by Z = -4 m, and a uniform beach with a slope of 1/20 and a berm height of h_R = 1 m were considered on the landward end. At the initial stage, a small random perturbation with an amplitude of ΔZ = 0.5 m was applied to the slope. The calculation domain was a rectangle of 4 km length and 1.2 km width, and a periodic boundary condition was set at both ends. In addition, the depth of closure was assumed to be h_c = 4 m. The equilibrium and repose slopes were 1/20 and 1/2, respectively. The coefficients of longshore and cross-shore sand transport were set to $K_s = K_n$ = 0.2, respectively. The calculation domain was divided with a mesh size of $\Delta x = \Delta y$ = 20 m, and Δt was selected to be 0.5 h. The total number of calculation steps considered was 5.5×10^4 (2.75×10^4 h). The calculation of the wave field was carried out every 10 steps in the calculation of beach changes. Table 1 shows the calculation conditions.

3.2. Calculation results

3.2.1. Oblique wave incidence from 60° counterclockwise

Figure 2 shows the results of the calculations at eight stages starting from the initial straight shoreline with a slope of 1/20, to which a small random perturbation with an amplitude of ΔZ = 0.5 m was applied, up to 5.5×10^4 steps. The small perturbation applied to the slope at the initial stage developed into eleven cuspate forelands within 5×10^3 steps, and the shoreline projection increased with time while moving rightward owing to the wave incidence from the counterclockwise direction. Because of the periodic boundary conditions at both ends, the cuspate forelands that moved away through the right boundary reentered the calculation domain through the left boundary. After 1×10^4 steps, the shoreline protrusion had increased and had developed as slender sand spits. After 2×10^4 steps, the small-scale sand spits located adjacent to each other had merged into large-scale sand spits and disappeared, and finally six sand spits were formed.

Two reasons for these changes are considered [1, 3]. (1) Of the two sand spits of different scales, the small sand spit moves faster than the large sand spit in the absence of the wave-sheltering effect, and then the small sand spit catches up and merges with the large sand spit. (2) On the lee of sand spits with an elongated neck, a wave-shelter zone is formed and the velocity of sand spits is reduced in this zone because of wave calmness, resulting in the stoppage of the movement of the sand spits and in the merging of small sand spits with larger spits.

Furthermore, the sand spits developed and protruded because (1) their tip is semicircular, meaning that the angle between the direction normal to the shoreline and the wave incident direction exceeds 45° at a point along the shoreline and the shoreline protrusion occurs at such a point owing to high-angle wave instability. (2) In a wave-shelter zone, sand transport is significantly reduced, whereas it is enhanced near the tip of the sand spits, and thus the derivative of the sand transport rate takes a maximum value near the boundary between the tip of the sand spits and the wave-shelter zone, inducing the protrusion of sand spits.

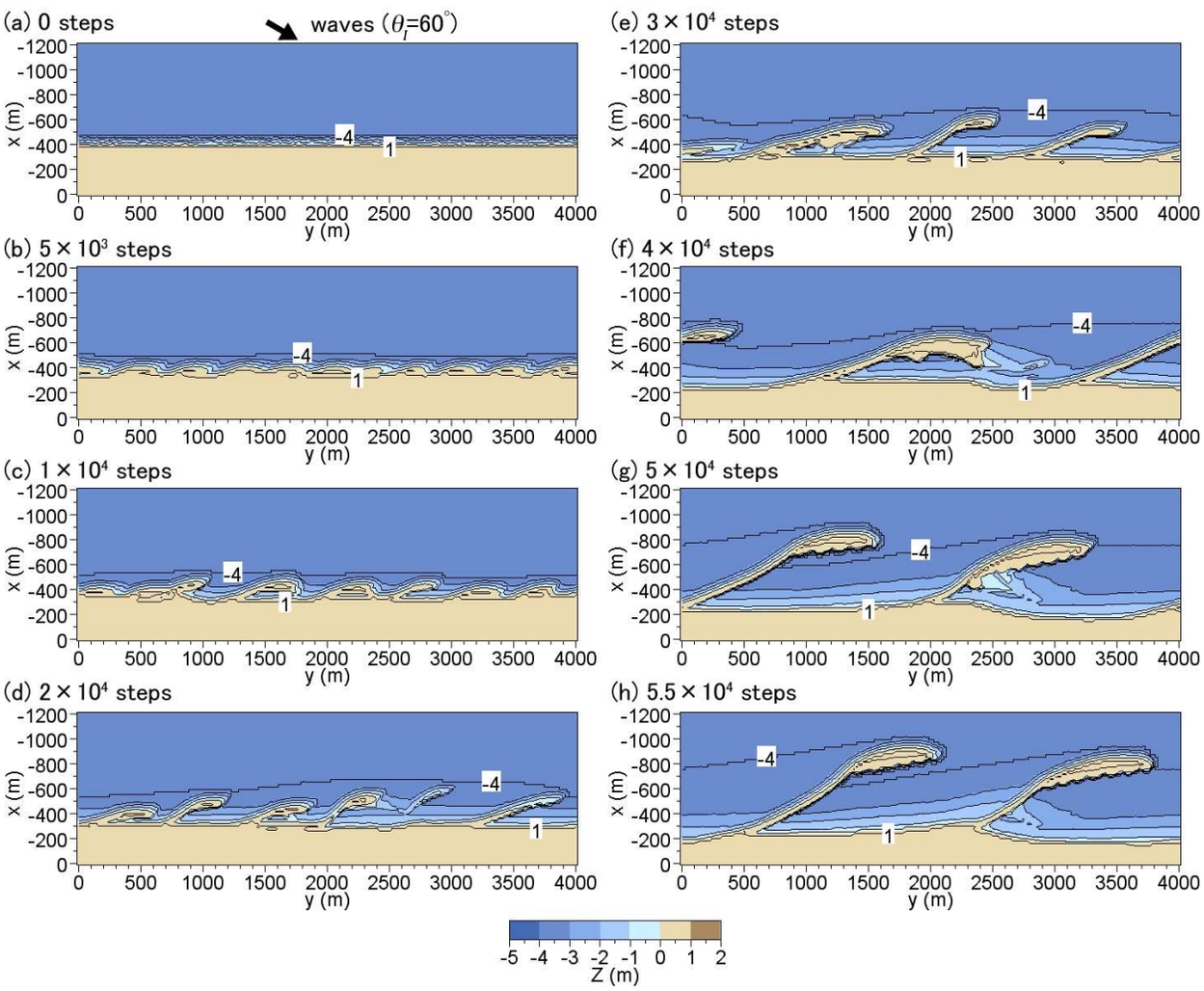

Figure 2. Development of sand spits from infinitesimal perturbation under wave conditions obliquely incident from 60° counterclockwise.

http://dx.doi.org/10.5772/57043

After 3×10^4 steps, the small sand spits located in the wave-shelter zone of the large-scale sand spits had stopped moving and merged into the large-scale sand spits, resulting in an increase in the interval between the sand spits and a decrease in the number of sand spits per finite length of the shoreline. After 4×10^4 steps, the number of sand spits had decreased to 2 and the tip of the sand spits approached closely to the original shoreline, permitting the downcoast passage of the sand of the sand spits.

After 5×10^4 steps, because of the movement of sand spits sweeping rightward, part of the sand deposition zone immediately offshore of the shoreline was left intact at the base of the sand spit located at y = 2250 m but almost all parts had merged with the sand spits. Although two large-scale sand spits were formed from the straight shoreline within 5.5×10^4 steps, the offshore contour of -4 m depth obliquely extended and a gentle seabed slope was formed upcoast of the sand spit, whereas a very steep slope was formed at the tip of the sand spits. These features are in good agreement with those measured around sand spits in lake and bay [18]. At the downcoast base of the sand spit extending from y = 2400 m, part of the sand bar formed in the previous process from 4×10^4 steps was left intact, implying that historical changes could be recovered at the downcoast side of the sand spit on the basis of the present topography.

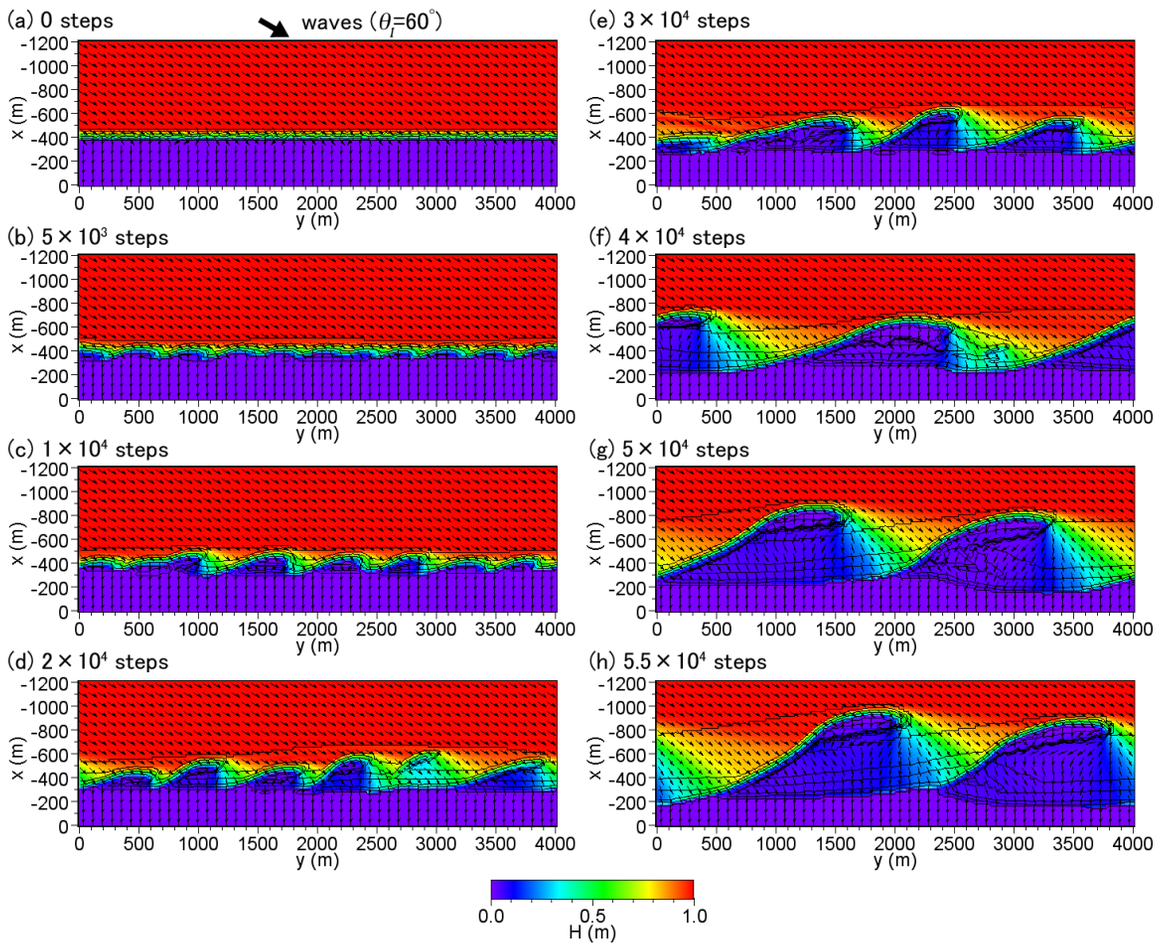

Figure 3. Change in wave field with development of sand spits.

Figure 3 shows the change in the wave field around the sand spits at each stage from the initial straight shoreline to the fully developed sand spits, as shown in Fig. 2. At the initial stage, waves are obliquely incident to the straight shoreline with uniform exposure to waves at all locations. With the development of the shoreline undulation over time, the wave-shelter zones were formed behind them. After 2×10^4 steps, the formation of sand spits was clear and the wave-shelter zone expanded downcoast, and the toe of the adjacent sand spit was included inside the wave-shelter zone. As a result, a marked reduction in wave height occurred, which in turn caused a reduction in sand transport. After 5.5×10^4 steps, long sand spits extended so that the toe of the slender sand spit was subject to the wave-sheltering effect of the upcoast sand spit. Owing to the development of sand spits over time, the entire original shoreline zone was included in the wave-shelter zone produced by sand spits, which is very similar to the calm wave zone protected by the extension of long port breakwaters.

Figure 4 shows the sand transport flux after 5.5×10^4 steps. The longshore sand transport mainly develops along the outer margin of the sand spit with a maximum value at the tip of sand spit and then rapidly decreases. Examining the sand transport flux near the neck of the sand spit in Fig. 4, cross-shore sand transport flux from the exposed side to the lee of the sand spit is also observed at a location of $y = 2750$ m. Thus, the neck of the sand spits is gradually eroded and moves downcoast because of this cross-shore sand transport, caused by the small difference between the given berm height h_R and the actual crown height of the sandy beach comprising the neck. Sand can be directly transported from the exposed side to the lee side without the sand transport turning around the tip of the sand spits. This effect makes the movement of an entire sand spit possible.

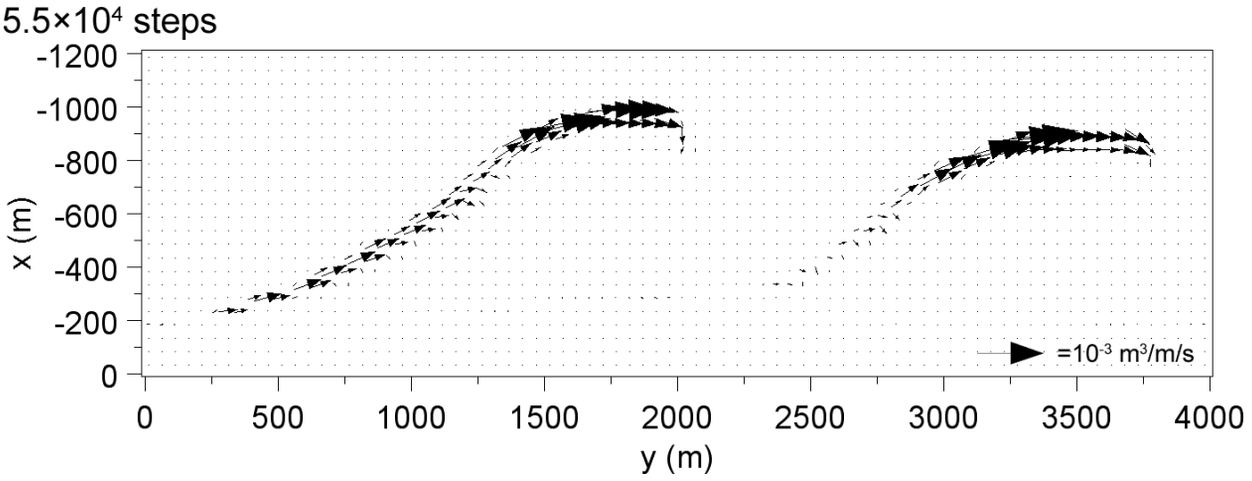

Figure 4. Sand transport flux after 5.5×10^4 steps.

3.2.2. Oblique wave incidence from 50° and 40° counterclockwise

In order to investigate the effect of the change in wave incidence angle to the beach changes, the calculations were carried out under the conditions of oblique wave incidence with an angle of 50° and 40°, while maintaining the same calculation conditions as in the case with an angle

http://dx.doi.org/10.5772/57043

of 60° except the wave incidence angle. Figure 5 shows the calculation results with an angle of 50°. The development of sand spits via the development of cuspate forelands owing to the instability mechanism was possible, but the scale of the sand spits was significantly reduced. However, no sand spits had developed at an angle of 40° and the shoreline undulations were smoothed out with time, as shown in Fig. 6, resulting that the shoreline undulations did not develop unless the wave incidence to the zone shallower than h_c exceeds 45°. This result agrees with the conclusion in [19] that the shoreline instability develops only if the bathymetric changes related to shoreline perturbations extend to a depth where the wave angle is greater than the critical angle of 42° and the potential for coastline instability is therefore limited by the wave incidence angle at the depth of closure and not the angle at deep water.

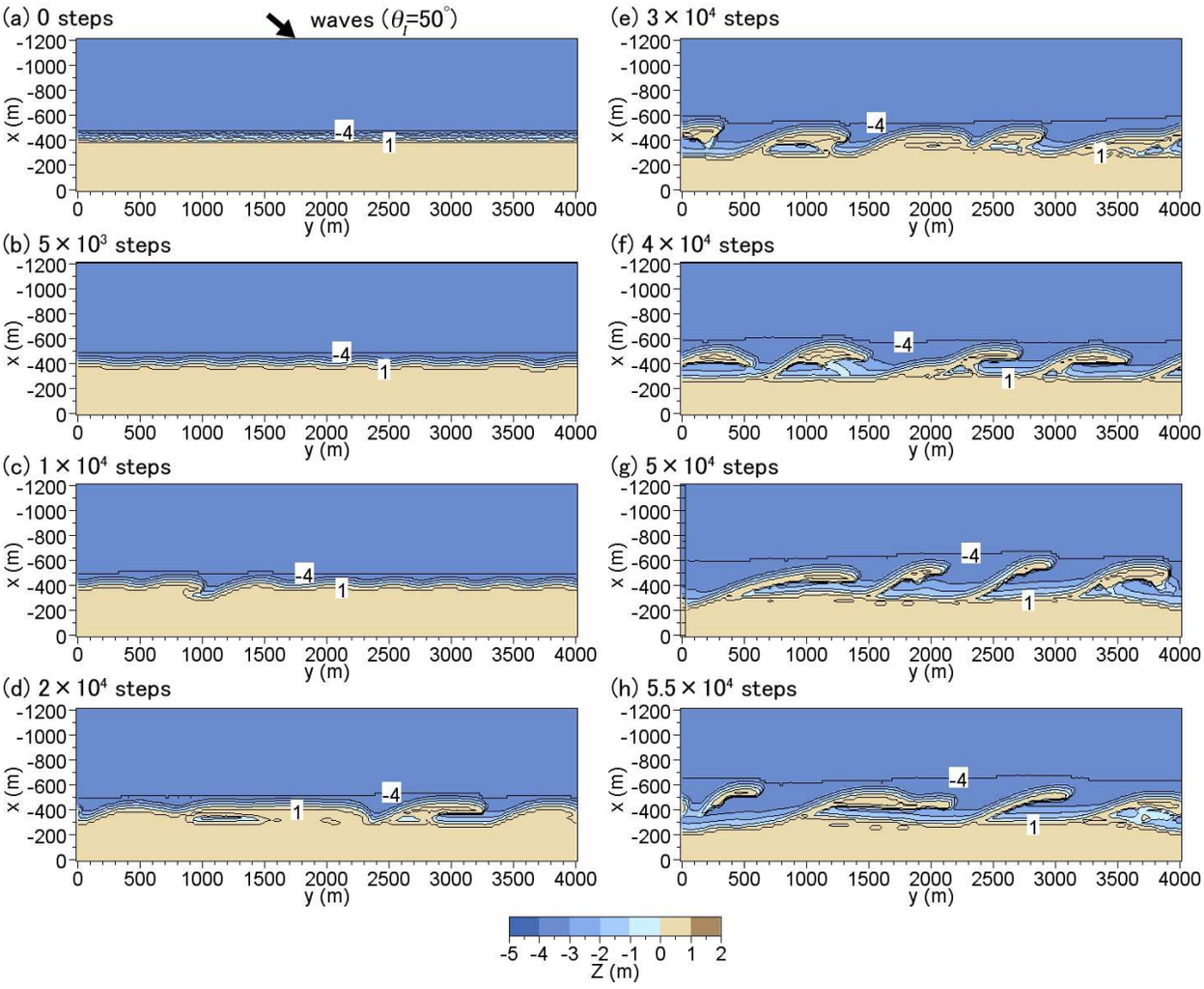

Figure 5. Formation of sand spits under the condition of oblique wave incidence from 50°.

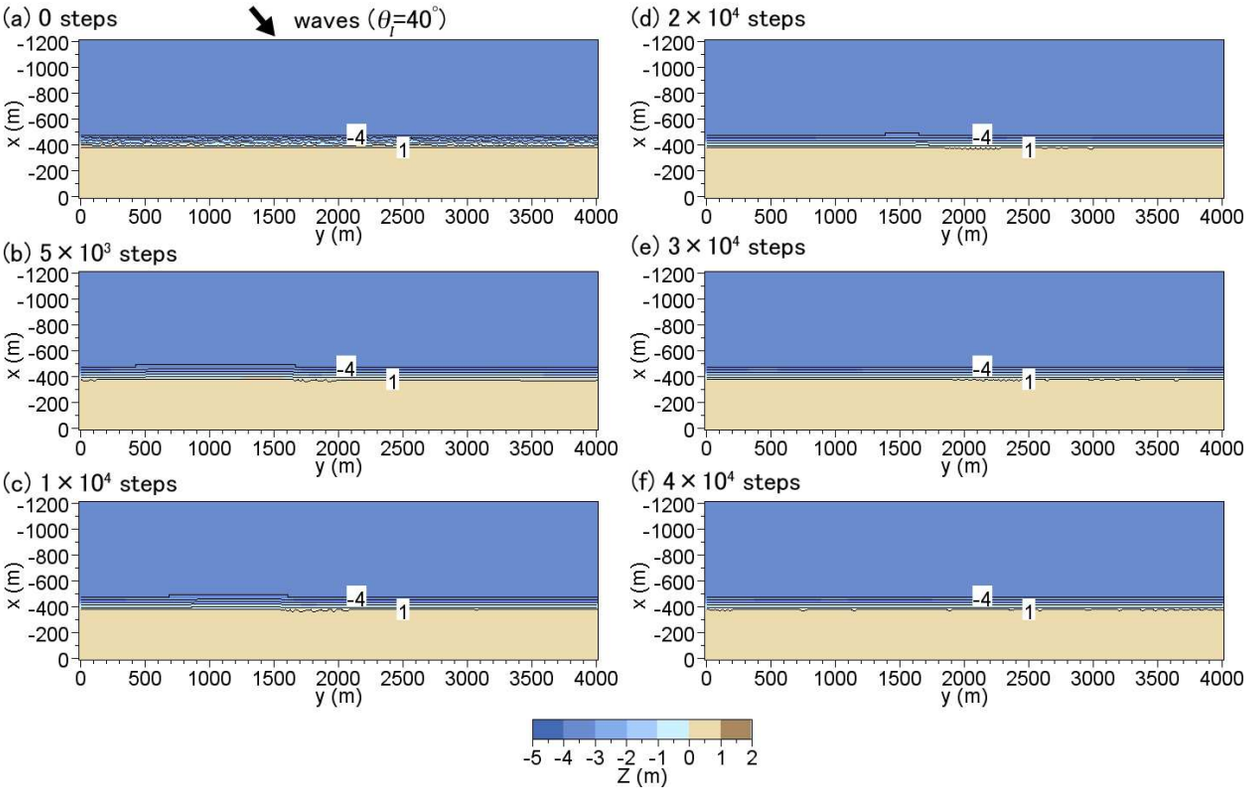

Figure 6. No shoreline instability under the condition of oblique wave incidence from 40°.

3.2.3. Oblique wave incidence from directions of ±60° with probabilities of 0.5:0.5

A numerical simulation was carried out for the case that waves were obliquely incident from the directions of ±60° relative to the direction normal to the shoreline with probabilities of 0.5:0.5 on the initial straight coastline, given a small random perturbation at the initial stage. Figure 7 shows the bathymetric changes between the initial stage and 4×10^4 steps. After 1×10^4 steps, triangular cuspate forelands had developed and irregularly distributed. When waves were incident from one direction, asymmetric sand bars developed, as shown in Fig. 2. In contrast, when waves with the same probability were incident from the opposite direction, the cuspate forelands became symmetric, and small-scale cuspate forelands disappeared and merged with larger cuspate forelands. Because the probability of occurrence of both wave directions was the same and there was no net longshore sand transport, the unidirectional movement of the sand body did not occur.

After 2×10^4 steps, the number of triangular cuspate forelands had been reduced to five, and the development of triangular cuspate forelands further continued and small-scale cuspate forelands merged into larger cuspate forelands. Finally, after 4×10^4 steps, four large-scale cuspate forelands had developed. A steep slope was formed by successive sand deposition at the tip of cuspate forelands, whereas seabed with a gentle slope was formed in the bay. Thus, when waves were obliquely incident from the directions of ±60° relative to the direction normal to the shoreline with probabilities of 0.5:0.5, symmetric cuspate forelands were formed.

http://dx.doi.org/10.5772/57043

Figures 8(a) and 8(b) show the wave height distribution around the cuspate forelands immediately after 4×10^4 steps under the conditions of clockwise and counterclockwise wave incidence. The wave-sheltering effect due to the protruded cuspate forelands alternately extends to the bays. The importance of this effect to the development of shoreline undulations was pointed out in [3]; when the multiple cuspate forelands with a different size have developed, the effect of the high-angle wave instability becomes stronger at the tip of the forelands with a large size than that at the bays, so that the positive feedback will occur. In contrast, around the cuspate forelands with a small size, the effect of the high-angle wave instability is weakened by the wave-sheltering effect by the large cuspate forelands, and the cuspate forelands are gradually modified to a stable form. Furthermore, when a large cuspate foreland develops, sand composed of the small cuspate foreland is absorbed into the large forelands, resulting in the decline of the small cuspate forelands and the increase in size of the large cuspate forelands. Thus, the development of large cuspate forelands will continue while small cuspate forelands are gradually disappearing. This results in the decrease in the number of the cuspate forelands.

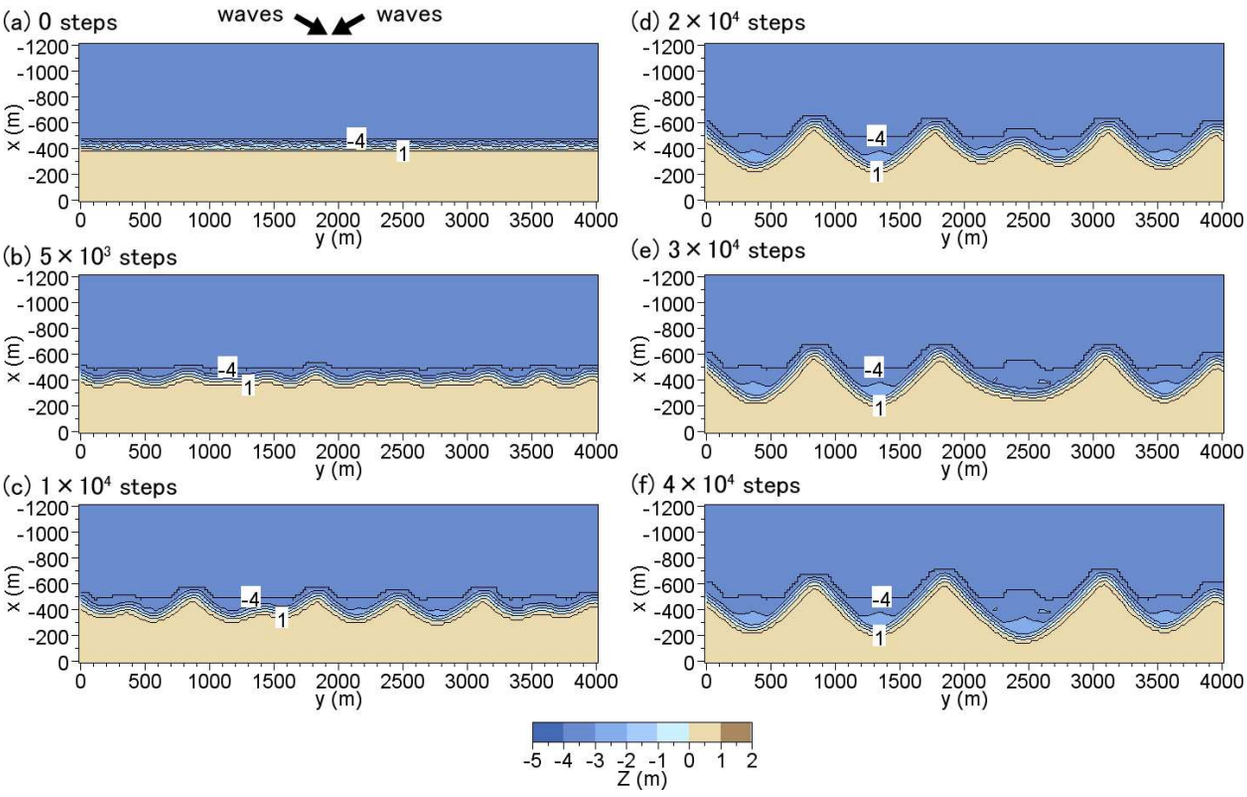

Figure 7. Formation of cuspate forelands (oblique wave incidence from ±60° with probabilities of 0.50:0.50).

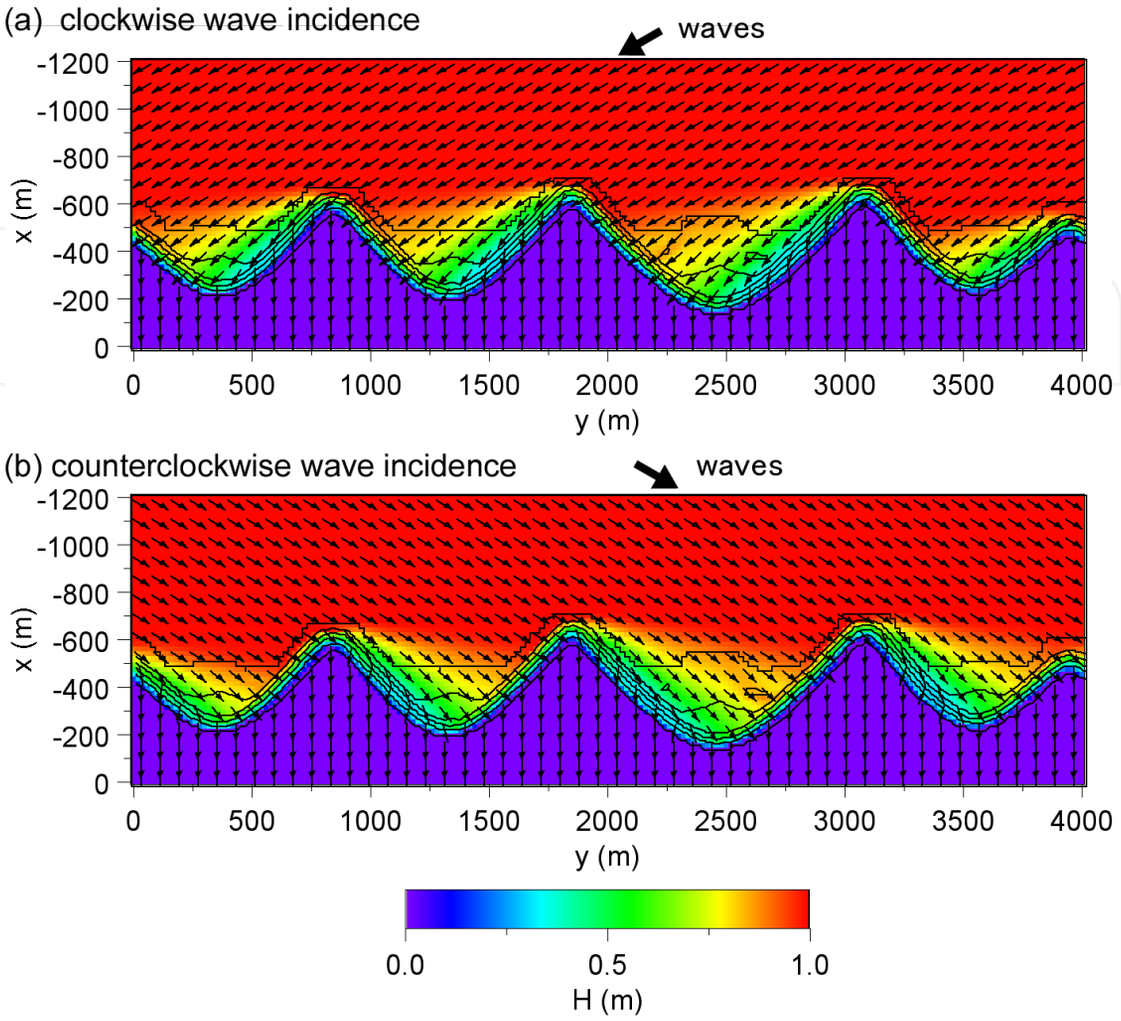

Figure 8. Wave field around cuspate forelands under oblique wave incidence from ±60° with probabilities of 0.50:0.50.

3.2.4. Oblique wave incidence from directions of ±60° with different probabilities

To investigate the effect of the change in probabilities of occurrence of the oblique wave incidence to the development of sand spits and cuspate forelands, the calculation was made, while keeping oblique wave incidence from directions of ±60° relative to the direction normal to the shoreline, and changing probabilities among 0.60:0.40, 0.65:0.35, 0.70:0.30, 0.75:0.25 and 0.80:0.20, i.e., the condition that rightward longshore sand transport gradually increases with the change in probability. In each case, the results after 2×10^4, 3×10^4 and 4×10^4 steps were compared.

Figure 9 shows the calculation results with probabilities of 0.60:0.40. Although symmetric cuspate forelands have developed with probability of 0.50:0.50, as shown in Fig. 7, asymmetric cuspate forelands that slightly inclined rightward have developed with probabilities of 0.60:0.40. Because the direction of net longshore sand transport was rightward, cuspate forelands developed while moving rightward. The shoreline left of the tip of cuspate forelands

http://dx.doi.org/10.5772/57043

extended straight, whereas the shoreline curvature increased immediately right of the tip, forming a hooked shoreline. The contour of 4 m depth extended toward the tip of the forelands while obliquely intersecting with the shoreline left of the tip of the foreland, and then it extended parallel to the shoreline from the tip of the foreland with a large curvature.

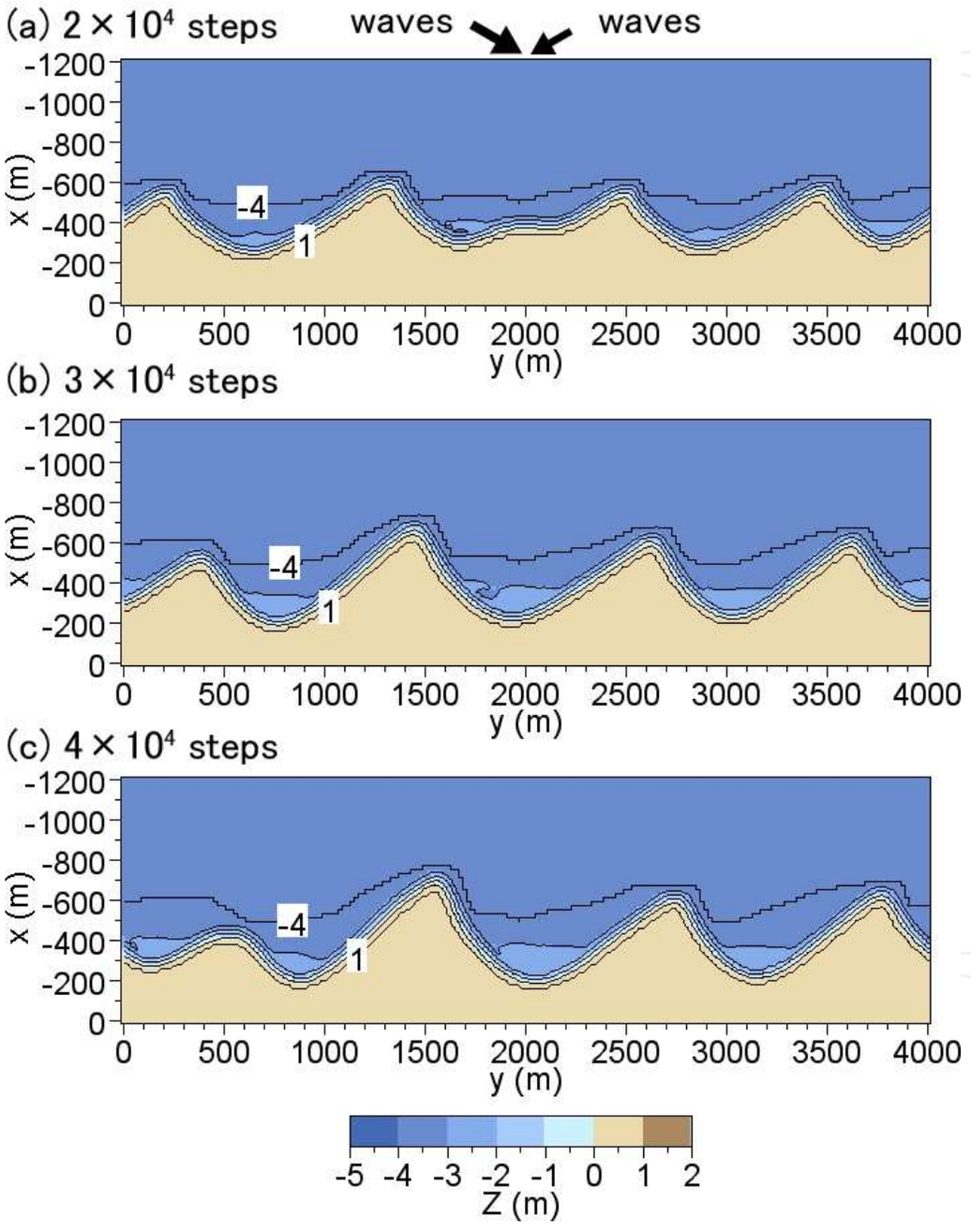

Figure 9. Formation of cuspate forelands (oblique wave incidence from ±60° with probabilities of 0.60:0.40).

Figure 10 shows the calculation results with probabilities of 0.65:0.35. Because probability of occurrence of wave incident from the left increased, the steepness of the cuspate forelands increased after 2×10^4 steps and a hooked shoreline inclined rightward had formed. After

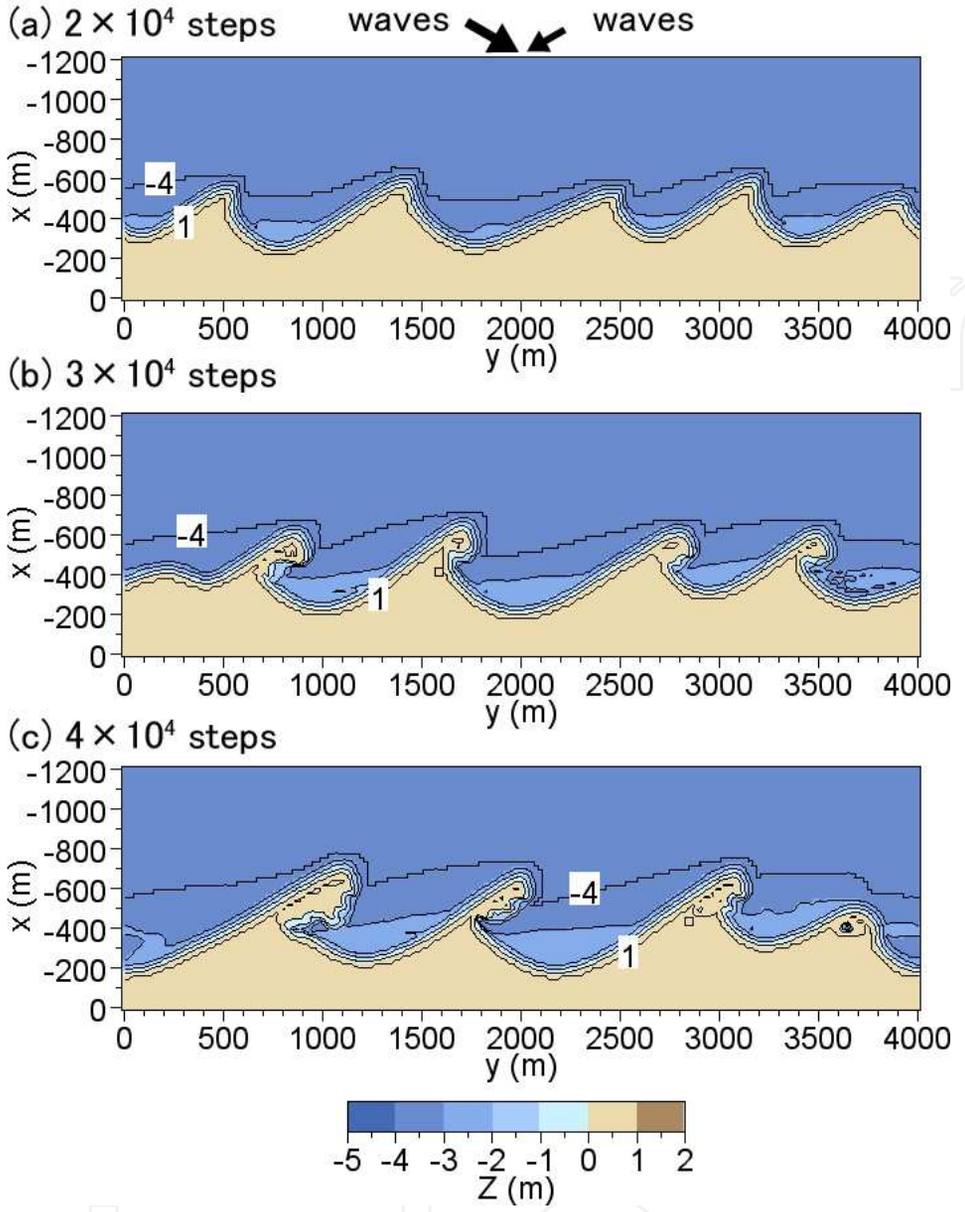

Figure 10. Formation of cuspate forelands (oblique wave incidence from ±60° with probabilities of 0.65:0.35).

3×10⁴ steps, sand spits were formed at the tip of the cuspate forelands and a shallow bay was formed between the apexes. After 4×10⁴ steps, sand spits obliquely extended rightward from the tip of the cuspate forelands with a larger angle than that in Fig. 2. In particular, the calculation results obtained after 4×10⁴ steps and the case in a lagoon facing Chukchi Sea shown in Fig. 1 are in good agreement.

Figure 11 shows the calculation results with probabilities of 0.70:0.30. Although sand spits had already developed after 2×10⁴ steps, these sand spits further elongated downcoast after 3×10⁴ steps, and after 4×10⁴ steps sand spits with a narrow neck at the connecting point to the land and a long head were formed. The number of the sand spits formed per unit coastline length reduced to two from four in the case with probabilities of 0.65:0.35.

http://dx.doi.org/10.5772/57043

Similarly, the calculation results with probabilities of 0.75:0.25 are shown in Fig. 12. A slender sand spit started to develop after 2×10^4 steps, and the sand spit with a narrow neck had elongated rightward after 3×10^4 steps. After 4×10^4 steps, sand spits with a long, slender neck and a head extended approximately parallel to the original coastline had developed. Although the contours shallower than 3 m depth extended parallel to the shoreline, while forming the main body of the sand spits, the contour of 4 m depth had an embayment downcoast of sand spits. Finally, Fig. 13 shows the calculation results with probabilities of 0.80:0.20. Because the probability of occurrence of waves from the left markedly increased, many sand spits with a head extended parallel to the original shoreline were formed close to the coastline after 2×10^4 steps. After 3×10^4 steps, the length of sand spits had further increased, but the head of sand spits extended parallel to the coastline similar to the development of longshore sand bars.

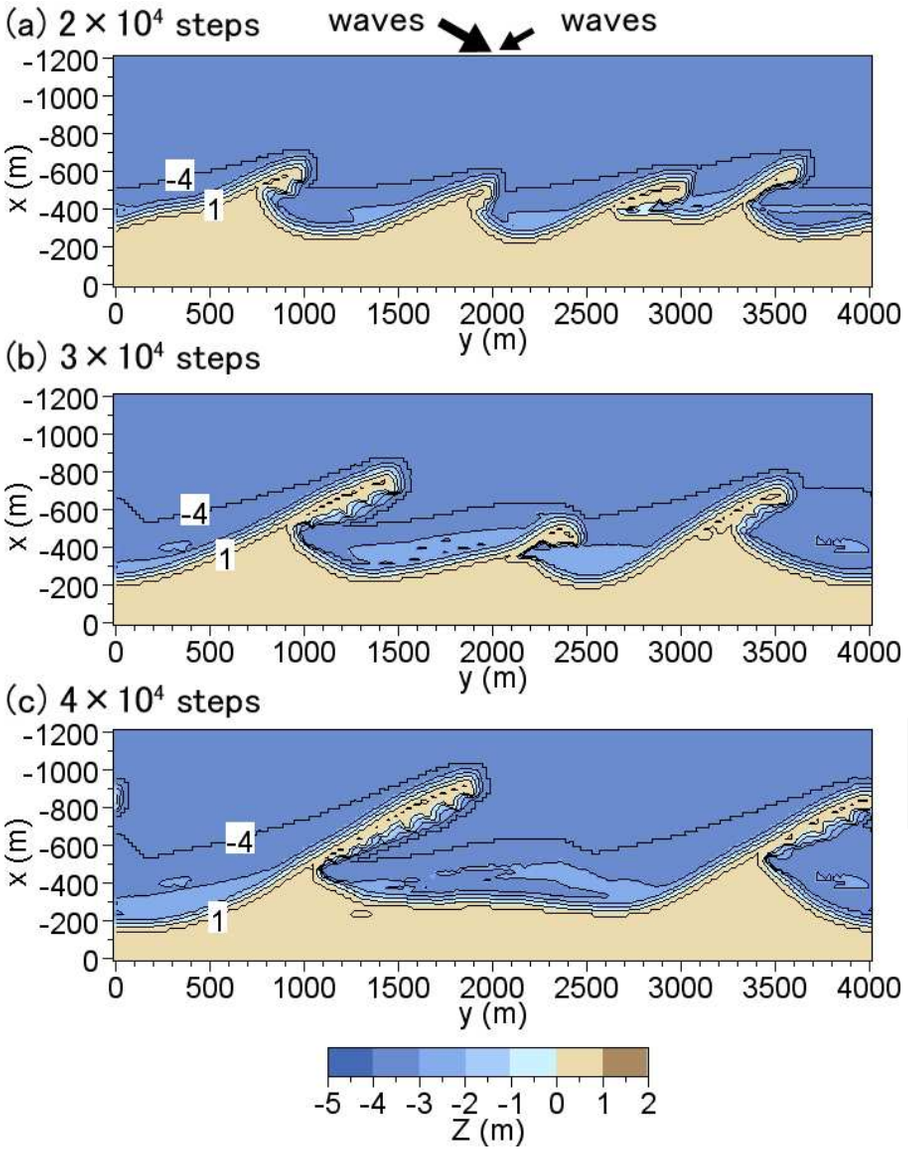

Figure 11. Formation of cuspate forelands (oblique wave incidence from ±60° with probabilities of 0.70:0.30).

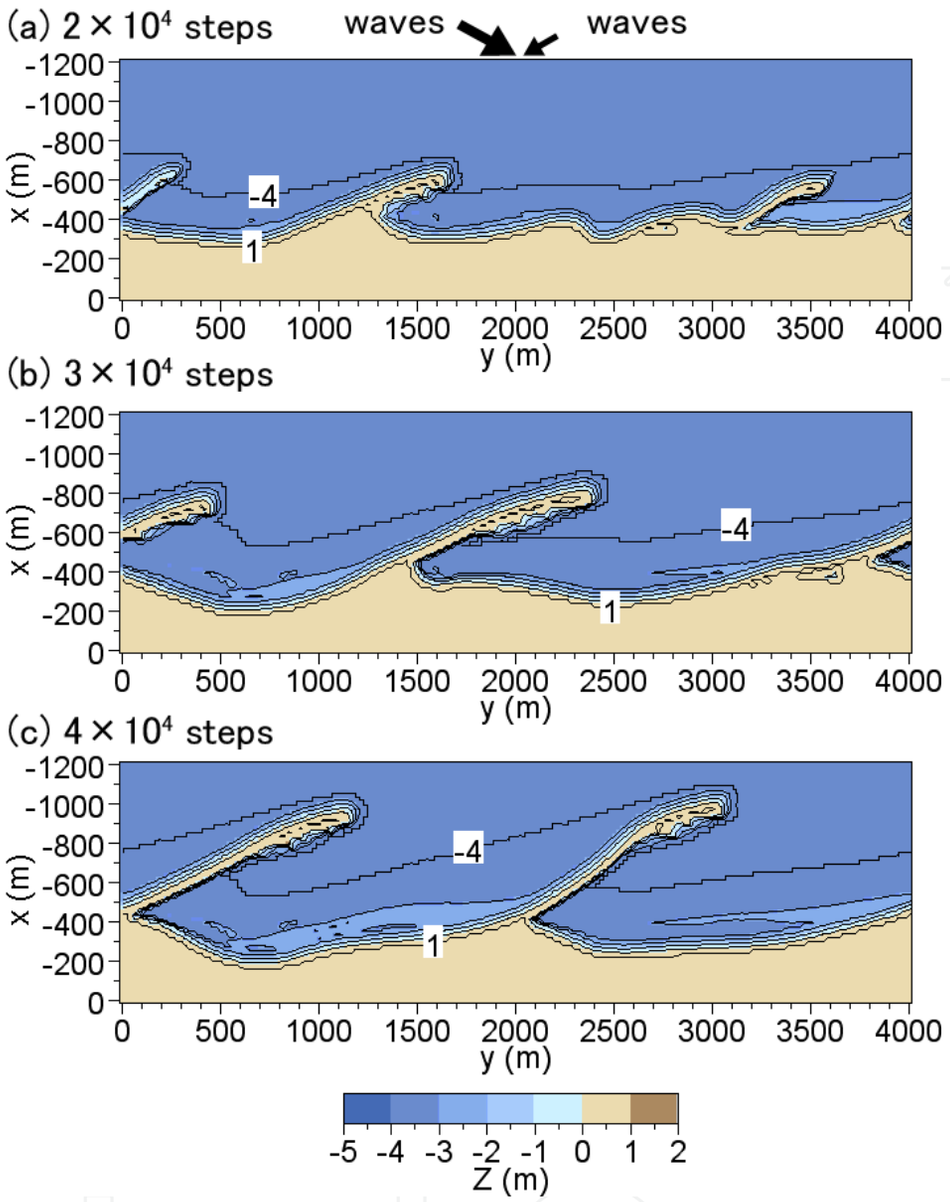

Figure 12. Formation of cuspate forelands (oblique wave incidence from ±60° with probabilities of 0.75:0.25).

Thus, symmetric cuspate forelands were formed when waves were incident from the directions of ±60° and the probability of occurrence of waves is equivalent. With probabilities of 0.60:0.40, the asymmetry of cuspate forelands increased and sand spits started to form after 2×10^4 steps with probabilities of 0.65:0.35. Increasing probabilities of occurrence of waves from the left such as 0.75:0.25, sand spits with a head extending parallel to the original shoreline developed. In all the cases of the development of sand spits, a narrow neck was formed at the connecting point to the land; a general characteristic of the topography around a sand spit [1]. Thus, the mechanism based on the high-angle wave instability and the evolution of 3-D beach changes was explained well by the BG model. Using this model, not only the shoreline configuration but also the 3-D topographic changes around the sand spits and cuspate forelands could be predicted.

http://dx.doi.org/10.5772/57043

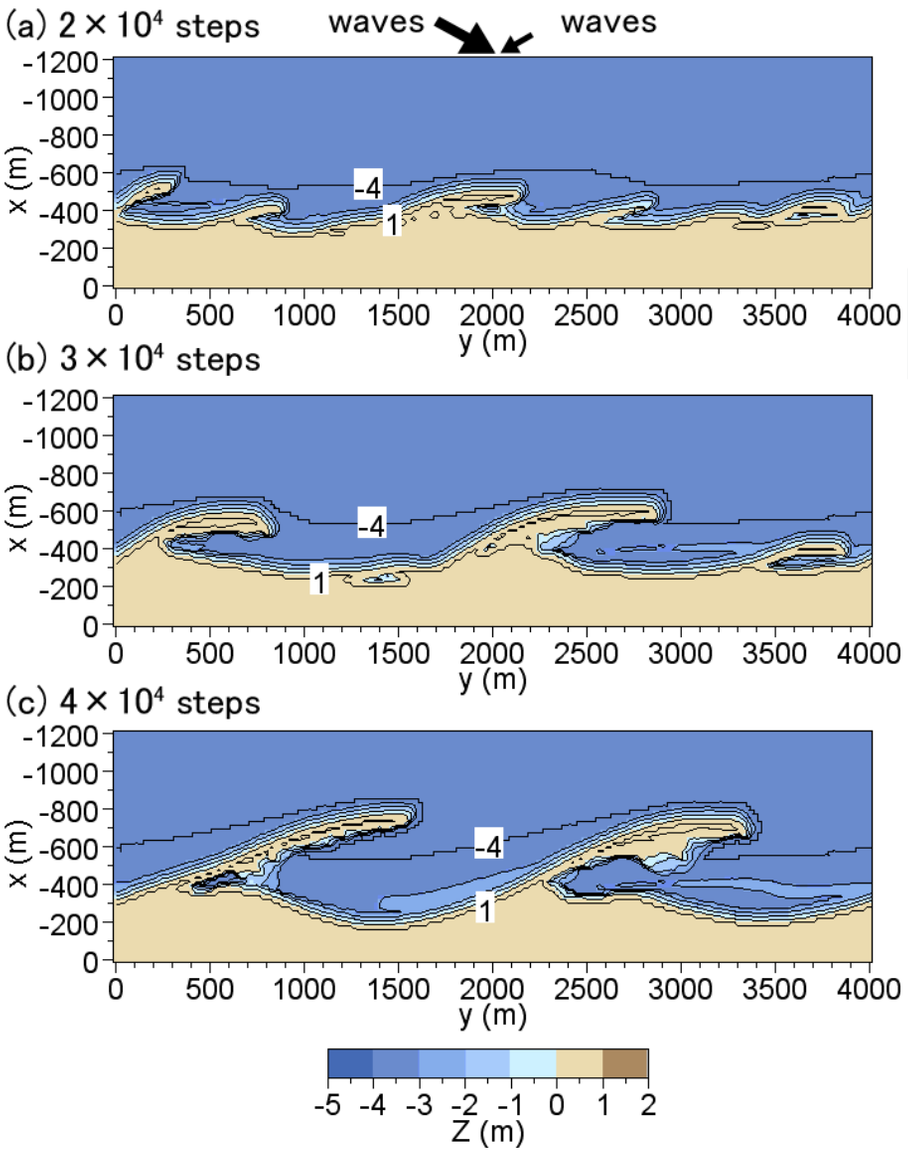

Figure 13. Formation of cuspate forelands (oblique wave incidence from ±60° with probabilities of 0.80:0.20).

3.3. Discussion

Although the scale of the sand spits formed along the north shore of the Azov Sea, as shown in Fig. 1, is much larger than that of the calculation results, their geometrical configurations of the calculated results are in good agreement with the measured. The sand spits A, B, C and D, as shown in Fig. 1, have been formed mainly by the waves obliquely incident from the east. The sand spit D located at the west end has a long, slender neck and this feature agrees well with the calculation results of the sand spit formed under the incidence of a unidirectional waves, as shown in Fig. 2(h). Furthermore, the width and length of the neck of the sand spit becomes thick and short in the order of C, B and A, along with the development of a hooked shoreline behind the sand spit. These conditions are very similar to the development of the sand spits under the conditions that waves were incident from two directions with different

probabilities. The shape of the sand spit A is very similar to that of the sand spit second from the right end in Fig. 10(c) calculated with probabilities of 0.65:0.35, and that of the sand spit C is similar to that located at right end in Fig. 11(b) calculated with probabilities of 0.70:0.30. On the north shore of the Azov Sea, easterly wind is considered to be predominant, and the sand spit D located at the west end could receive sufficiently large wave energy from the east because of long fetch, whereas wave action from the west is weak because of shorter fetch. As a result, wave action from the east became stronger and sand spit with a narrow, slender neck was considered to be formed. In contrast, in the sand spit A, the fetch from the east was short so that the wave action from the east was weakened, whereas wave action from the west was strengthened because of a long fetch. In addition, the increase in the fetch of the easterly wind was considered to cause the increase in scale of the sand spit. Zenkovich qualitatively explained these features using a schematic diagram [1], but in this study these features observed in the field were successfully explained using the BG model.

Falqués et al. [6] predicted the development of sand waves caused by high-angle wave instability using equations similar to that of our model. Their sand transport equation had the same stability mechanism as that in our model. However, because the calculation domain of the wave field was restricted between the offshore zone and the breaking point, they only predicted the development of sand waves but not the development of sand spits protruding offshore. In this study, wave decay in the breaker zone and the wave-sheltering effect by the sand spit themselves were evaluated, taking the local change in topography in the surf zone into account and using the energy balance equation for irregular waves.

4. Effects of anthropogenic factors on development of sand spits and cuspate forelands

4.1. General conditions

The formation of sand spits and cuspate forelands with rhythmic shapes has already predicted in Chapter 3. Here, we investigated the effects of the construction of a groin and a breakwater to the topographic changes in the field where sand spits and cuspate forelands with rhythmic shapes fully developed. All the calculation conditions were the same as those in Chapter 3 except the structural conditions. Five calculations were carried out with the installation of a groin of 800 m length or an offshore breakwater of 600 m or 1000 m length.

In Cases 1 and 2, a groin or a breakwater was placed at the center of the calculation domain, respectively, after the development of sand spits under the condition that waves were obliquely incident from the left with an angle of 60°, as shown in Fig. 2. In Cases 3 and 4, in which waves are incident with an angle of ±60° with probabilities of 0.5:0.5, as shown in Fig. 7, a breakwater was placed offshore of the apex or the bay of the cuspate forelands, respectively. In Case 5, a breakwater was installed under the condition that waves are incident with an angle of ±60° with probabilities of 0.65:0.35, as shown in Fig. 10. The wave direction was randomly determined on the basis of the probability distribution at every step of the calculation of the

http://dx.doi.org/10.5772/57043

wave field. The lengths of the groin and breakwater were determined, taking both the scale of sand spits and cuspate forelands and the wave diffraction effect of the structures into account. The calculation with no structures was carried out up to 3×10^4 steps, and then the beach changes up to an additional 3×10^4 steps were predicted after the installation of the structures.

4.2. Calculation results

4.2.1. Effect of groin on formation of sand spits

The beach changes until 3×10^4 steps were calculated under the conditions that waves are obliquely incident from the direction of 60° and then a groin of 800 m length and 4 m point depth was installed across the central sand spit after the sand spits have fully developed owing to the shoreline instability (Fig. 14(a)). These sand spits have developed while moving rightward, and the sand spit that moved out of the right boundary enters again from the left boundary as it is because of the periodic boundary condition at both ends. Figures 14(b)-14(j) show the results.

After 2×10^3 steps, the sand spit located left of the groin connected to the groin with a lagoon inside, whereas erosion started right of the groin because rightward longshore sand transport was obstructed by the groin. After 4×10^3 steps, part of the sand blocked by the groin started to be transported to the right while turning around the tip of the groin. The same situation continued after 6×10^3 steps, and a sand spit was formed owing to the deposition of sand turning around the tip of the groin up to 8×10^3 steps. Furthermore, as a result of sand discharge to the area right of the groin between 4×10^3 and 8×10^3 steps, the volume of sand left of the groin decreased, and the location of the starting point P of sand bar approached the groin with time, resulting in the decrease in the scale of the lagoon behind the sand bar.

Until 1×10^4 steps, the sand spit formed at the tip of the groin elongated rightward along with the reduction in the scale of the sand bar left of the groin. After 1.5×10^4 steps, the sand spit extending from the tip of the groin became a flying spit [20, 21] because of the reduction in sand supply by longshore sand transport. Because the flying spit is an unstable topography, it rapidly disappeared until 2×10^4 steps. Then, because of the increased sand supply owing to the connection of another sand spit to the groin, a sand spit elongated obliquely from the tip of the groin until 3×10^4 steps. It was realized from the comparison of Figs. 14(a) and 14(j) that sand was deposited, forming a steep slope along the shoreline on the exposed side, but the water depth generally decreased in the offshore zone owing to the sweeping motion of the sand spit, causing offshore sand movement. In contrast, sandy beach with a gentle slope was formed in the lee of the sand spits and six branches were formed behind the sand spit. The longshore sand transport was pushed seaward by the construction of a groin.

4.2.2. Effect of breakwater on formation of sand spits

The beach changes until 3×10^4 steps were calculated under the conditions that waves were obliquely incident from the direction with an angle of 60° to the direction normal to the shoreline, and then a breakwater of 600 m length was installed offshore of sand spit A after

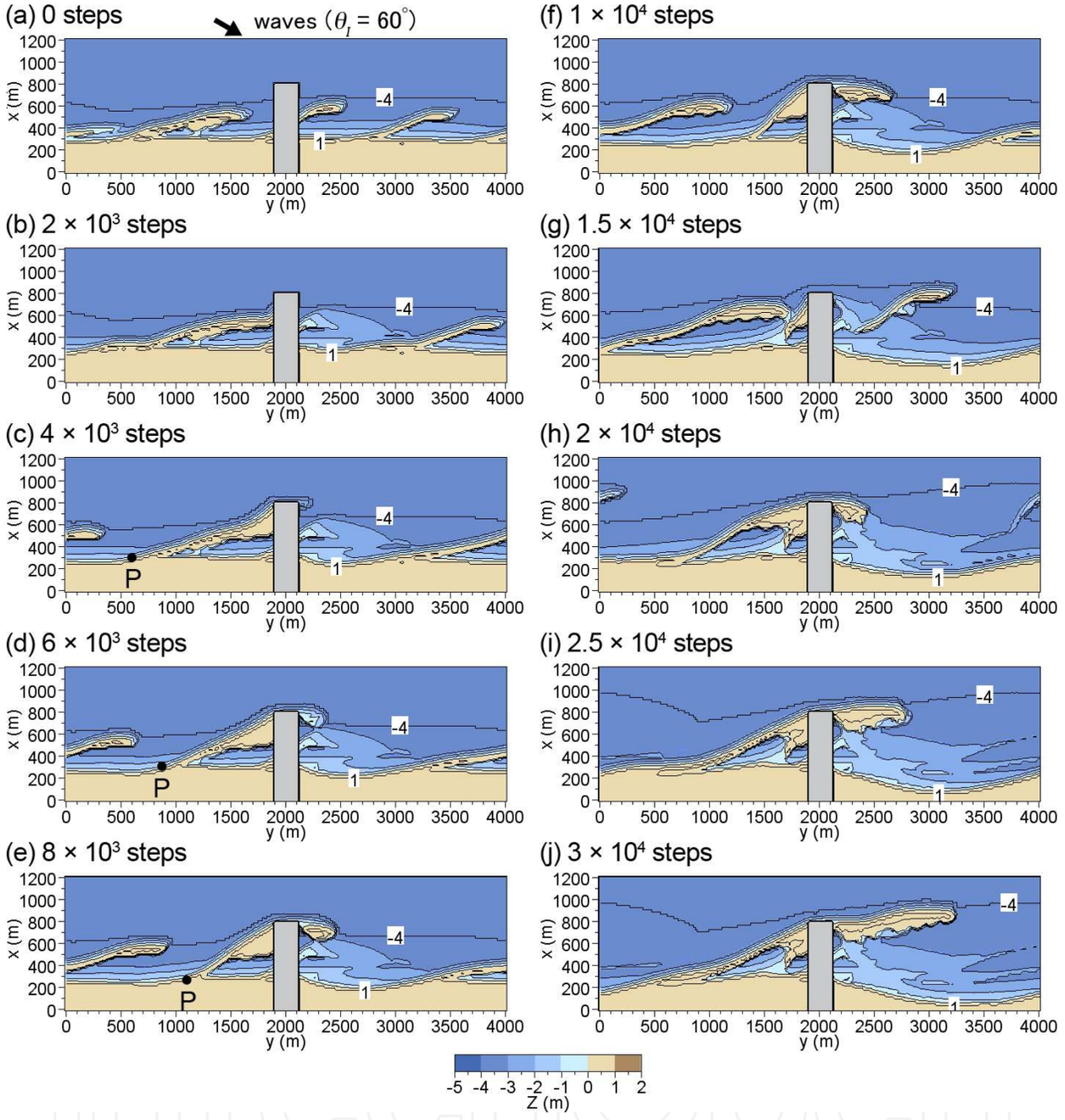

Figure 14. Deformation of sand spits formed under oblique wave incidence from 60° after extension of a groin.

the full development of sand spits owing to the high-angle wave instability (Fig. 15(a)). The beach changes were further calculated until 3×10⁴ steps, as shown in Figs. 15(b) - 15(j).

After 2×10³ steps, sand spit A behind the breakwater was eroded, because it was fully included in the wave-shelter zone of the breakwater, as shown in Fig. 16(a), and the wave height was significantly reduced with the change in wave direction, resulting in the reduction in rightward longshore sand transport. In contrast, sand spit B elongating left of the lee of the breakwater rapidly extended to the lee of the breakwater because of large longshore sand transport, as

http://dx.doi.org/10.5772/57043

shown in Fig. 16(a). The same situation continued after 4×10^3 steps and the rest of the sand of sand spit A was obliquely transported landward, and sand spit A disappeared while leaving the outline of the sand spit. During the period, sand spit B further extended to the lee of the breakwater. The change in wave field corresponding to this stage is shown in Fig. 16(b). Although the tip of sand spit B is subjected to strong impact of waves diffracted from the left end of the breakwater, wave height is significantly reduced between the tip of sand spit B and the breakwater, thus the tip of sand spit B extended so as to approach the breakwater.

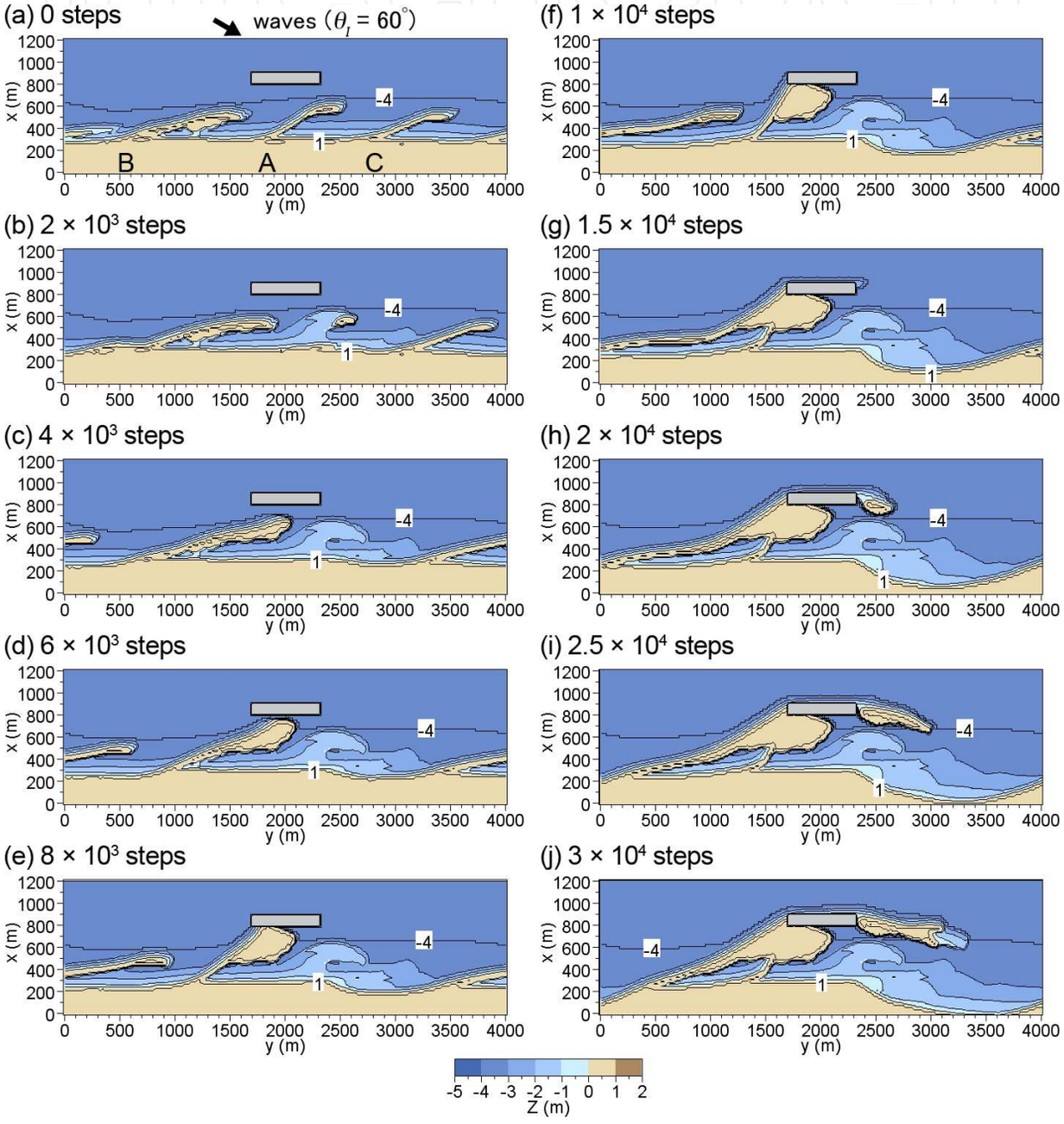

Figure 15. Deformation of sand spits formed under oblique wave incidence from 60° after construction of a breakwater.

The beach changes continued up to 6×10^3 steps and the volume of sand deposited behind the breakwater increased along with the shoreline recession downcoast of the breakwater, as shown in Fig. 15(d). After 8×10^3 steps, a large tombolo was formed by the trapping of sand. After 1×10^4 steps, another sand spit, which elongated from the left end, extended to connect the tombolo behind the breakwater. After 1.5×10^4 steps, a continuous sand bar developed from the left end to the breakwater. Then, a small sand spit started to emerge at the right end of the breakwater by 2×10^4 steps. After 3×10^4 steps, the sand spit extended from the right end of the breakwater further elongated, even though the volume of sand deposited behind the breakwater did not change. Thus, the construction of the breakwater had a significant impact on the beach; otherwise, sand spits developed with the self-organization mechanism, as shown in Fig. 2. It is realized that once a tombolo is formed behind the breakwater, offshore sand movement is enhanced owing to the presence of the breakwater and the tombolo, which blocks longshore sand transport.

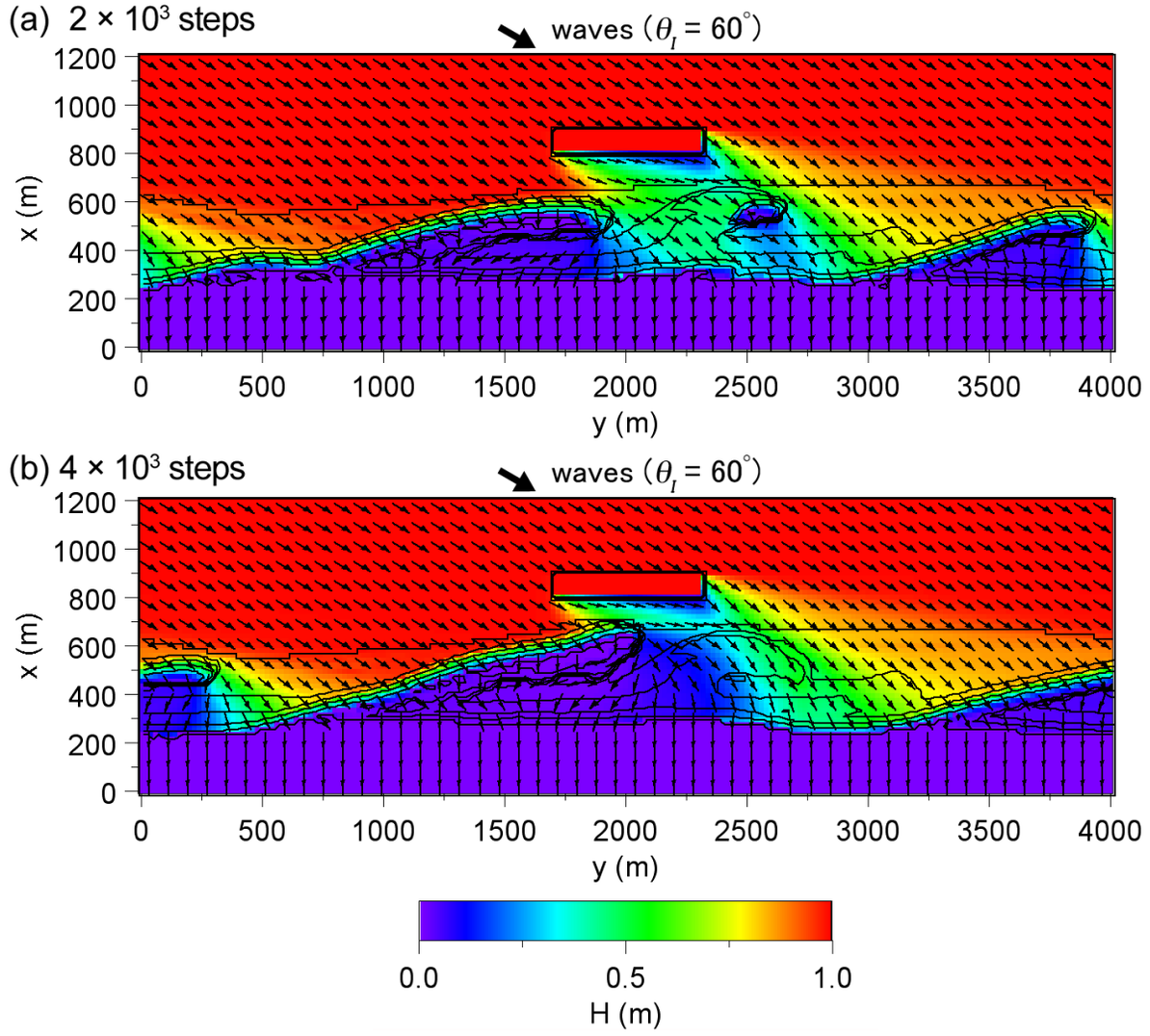

Figure 16. Wave field around a breakwater after 2×10^3 and 4×10^3 steps.

http://dx.doi.org/10.5772/57043

4.2.3. Effect of breakwater placed offshore of apex of cuspate forelands

When waves were obliquely incident with an angle of ±60° to the direction normal to the shoreline with the probability of 0.5:0.5, cuspate forelands have developed by 3×10^4 steps, as shown in Fig. 7. This bathymetry was selected as the initial topography, as shown in Fig. 17 (a). Here, the cuspate foreland formed at the center is designated as A along with cuspate forelands B and C on the left and right, respectively. Then, a breakwater of a 1000 m length was placed offshore of cuspate foreland A, and the calculation was made until 4×10^4 steps. Results are shown in Fig. 17(b) - 17(h).

Under these conditions, approximately symmetric wave-shelter zone was formed on both sides of the breakwater. The slender sand spits started to extend toward the lee of the breakwater near the tip of cuspate forelands B and C after 5×10^3 steps, as shown in Fig. 17(b). These sand spits were asymmetric with the sand spit being larger size at cuspate foreland B. Figure 18 shows the wave field after approximately 5×10^3 steps when waves are incident from the right and left, for example. Because the breakwater is placed offshore of cuspate foreland A and the distance between cuspate forelands A and B is shorter than that between cuspate forelands A and C, cuspate foreland B is subjected to an intensive wave-sheltering effect by the breakwater and cuspate foreland A under the condition that waves are incident from the right, whereas cuspate foreland C is located outside the wave-shelter zone by the breakwater and cuspate foreland A under the conditions that waves are obliquely incident from the left. Thus, the intensive wave-sheltering effects by the breakwater appeared at cuspate foreland B, resulting in the increase in the formative velocity of the sand spit near the tip of the cuspate forelands.

Furthermore, in Fig. 17(b), cuspate foreland A protruded more than that under the initial condition. The same changes continued until 1×10^4 steps with rapid elongation of the sand spit at the tip of cuspate foreland B to the lee of the breakwater and it almost connected to cuspate foreland A. On the other hand, cuspate foreland C was started to be eroded because of the leftward development of the sand spit at the tip of the cuspate foreland.

After 1.5×10^4 steps, the sand spit elongated from the tip of cuspate foreland B connected to cuspate foreland A and a barrier was formed with a lagoon inside. The scale of the sand spit formed at the tip of cuspate foreland C also increased, and the shoreline curvature increased downcoast of the sand spit C because of the wave-sheltering effect of the sand spit itself. After 2×10^4 steps, cuspate foreland B was entirely eroded, leaving a barrier island with a straight shoreline and a tombolo was formed behind the breakwater. No beach changes occurred inside the lagoon since then. On the right side of the breakwater, a sand spit elongated leftward with many branches to cuspate foreland A. After 2.5×10^4 steps, the tombolo behind the breakwater further developed and the beach width was widened up to 240 m behind the breakwater. Furthermore, the sand spit extended leftward from the tip of the cuspate foreland C connected to the cuspate foreland A and a lagoon was formed behind the barrier. Finally, after 4×10^4 steps, a large tombolo was formed with two water bodies inside the sandy beach behind the breakwater, the cuspate forelands with rhythmic shapes, as shown in Fig. 17(a), markedly deformed, and marked beach changes were induced by the wave-sheltering effect of the breakwater.

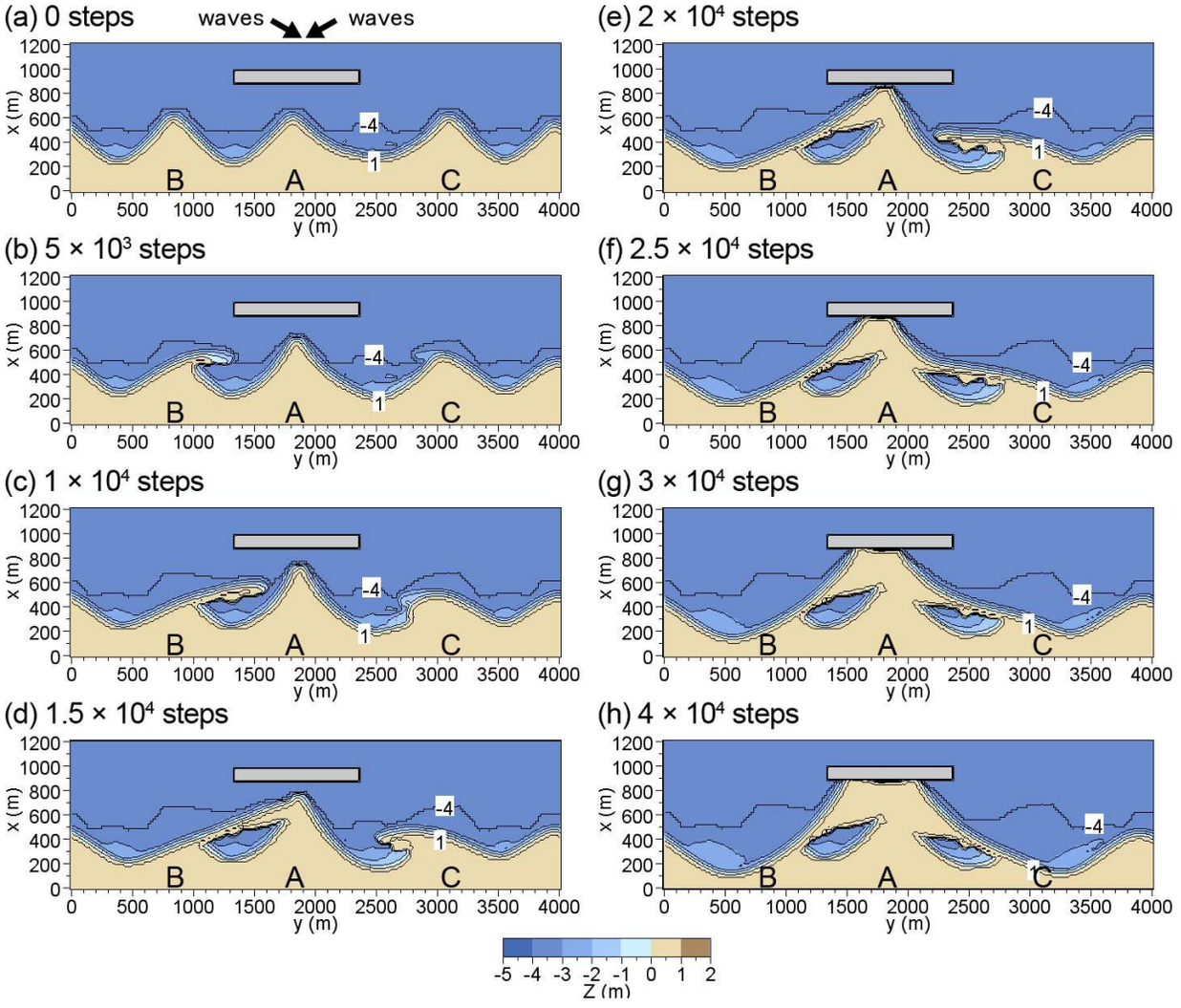

Figure 17. Deformation of cuspate forelands formed under the condition of oblique wave incidence from ±60° with probabilities of 0.5:0.5 after construction of a breakwater offshore of apex of cuspate foreland A.

4.2.4. Effect of breakwater placed offshore of bay of cuspate forelands

To investigate the topographic changes caused by the difference in the wave-sheltering effect which was produced by the change in location of the breakwater, the location of the breakwater was altered from offshore of the apex in the former case to offshore of the bay of the cuspate forelands. The same bathymetry shown in Fig. 17(a) with four cuspate forelands was selected as the initial bathymetry (Fig.19(a)), and an impermeable breakwater of a 1000 m length was placed offshore of a bay between the cuspate forelands A and B. Beach changes until 4×10^4 steps were predicted under the condition that waves were incident with an angle of ±60° to the direction normal to the shoreline with probabilities of 0.5:0.5. Figures 19(b) - 19(h) show the results.

In this case, almost half of the cuspate forelands A and B were included in the wave-shelter zone of the breakwater. Because of the symmetry of the location of cuspate forelands A and B relative to the breakwater, the wave field also showed symmetry, so that a pair of sand spits

http://dx.doi.org/10.5772/57043

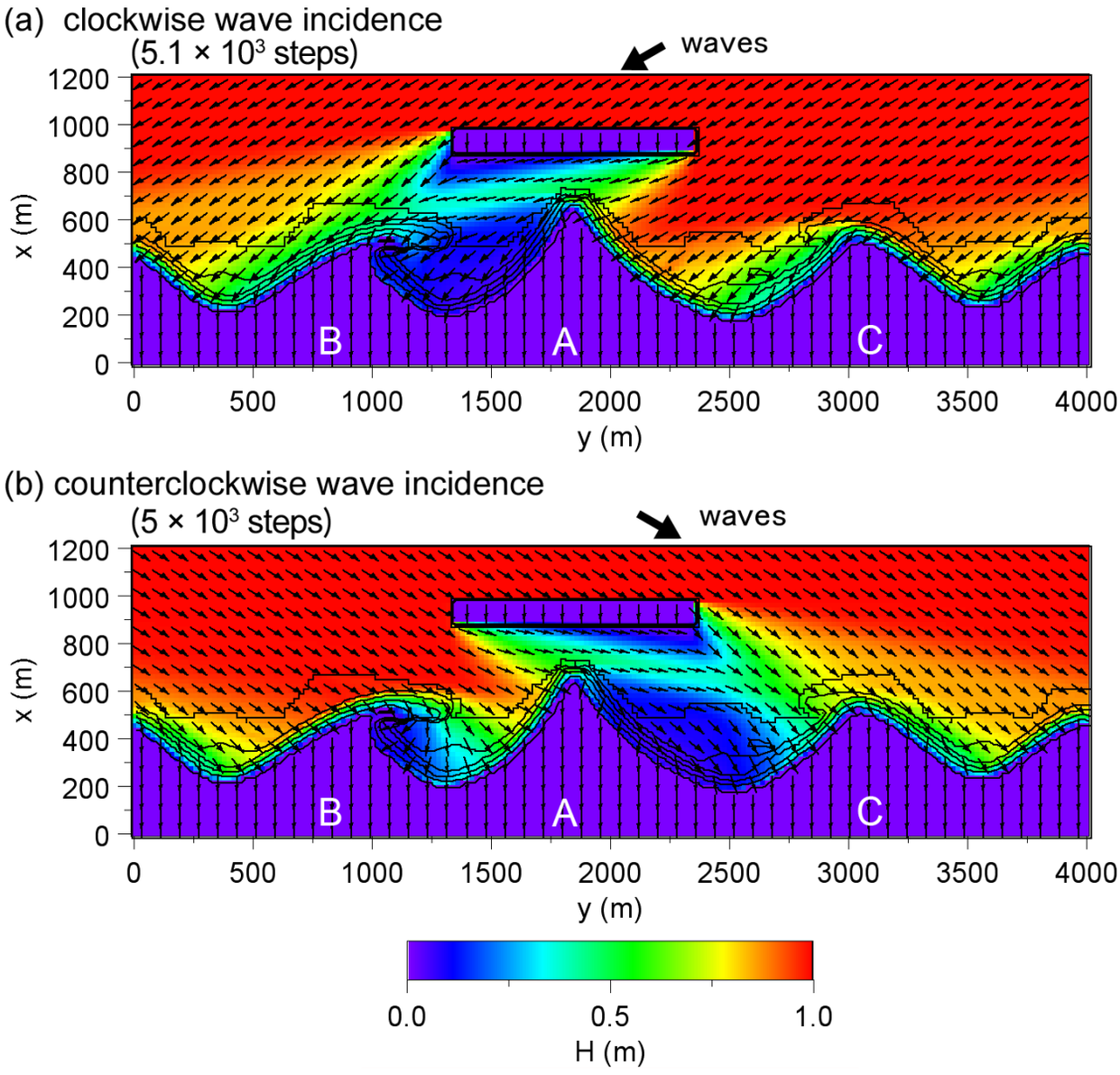

Figure 18. Wave field around a breakwater after 5.1×10^3 and 5×10^3 steps.

elongated toward the lee of the breakwater from the tip of the cuspate forelands until 5×10^3 steps, while enclosing a lagoon inside (Figs. 19(b) and 19(c)). The same changes continued after 1×10^4 steps and the sand spits extended from the tip of the cuspate forelands A and B were about to connect to the breakwater. After 1.5×10^4 steps, both sand spits connected to the breakwater, forming a double tombolo. After 2×10^4 steps, the double tombolo fully attached to the breakwater, and no beach changes occurred along the lagoon shore. With time, the double tombolo developed, resulting in increase in the size. Finally, the initial shape of the cuspate forelands with rhythmic shapes shown in Fig. 19(a) entirely disappeared. Comparing the beach topographies after 4×10^4 steps, as shown in Figs. 17(h) and 19(h), the number of lagoons enclosed inside the barrier was different; two in Fig. 17(h) and one in Fig. 19(h), although double tombolo developed in both cases.

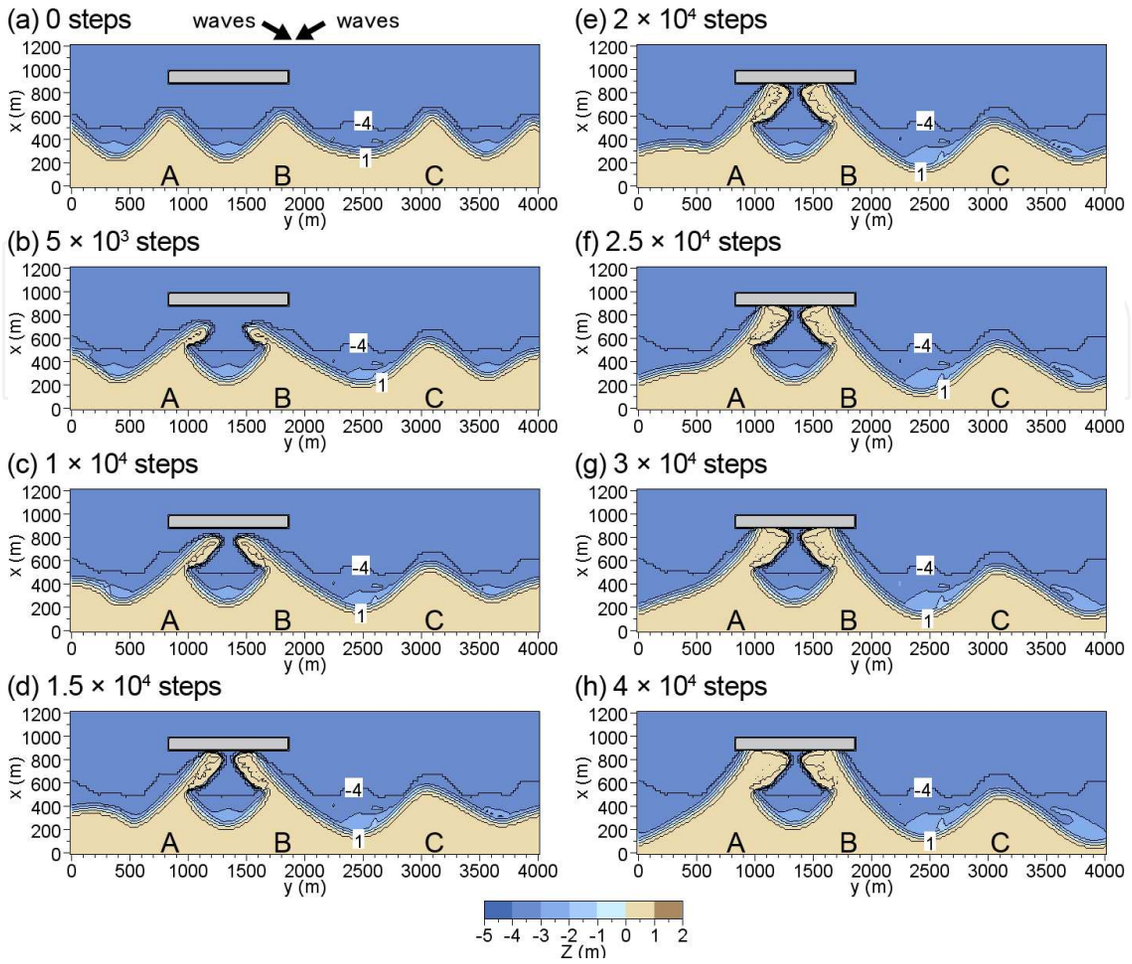

Figure 19. Deformation of cuspate forelands formed under the condition of oblique wave incidence from ±60° with probabilities of 0.5:0.5 after construction of a breakwater offshore of bay of cuspate forelands.

4.2.5. Effect of breakwater on formation of asymmetric sand spits

In this case, sand spits with asymmetric shapes were formed first under the condition that waves were obliquely incident from the direction of ±60° normal to the shoreline with probabilities of 0.65:0.35, as shown in Fig. 10. Then, an offshore breakwater of a 600 m length (the same condition as that shown in Fig. 15) was constructed in a zone offshore of sand spits A and B, and beach changes were calculated until 4×10^4 steps. The calculation results are shown in Figs. 20(a)-20(h).

Figure 21 shows the wave field after approximately 5×10^3 steps when waves were obliquely incident from the right and left. Because not only the probability of each wave direction was not equal as 0.65:0.35 but also sand spit B was located closer to the breakwater than sand spit C, an extremely asymmetric wave field was formed. Sand spit C was barely subjected to the wave-sheltering effect by the breakwater, whereas sand spit B effectively entered into the wave-shelter zone of the breakwater under the wave incidence from the left. Moreover, sand spit A was subjected to receive a strong wave-sheltering effect by the breakwater because of its proximity to the breakwater.

http://dx.doi.org/10.5772/57043

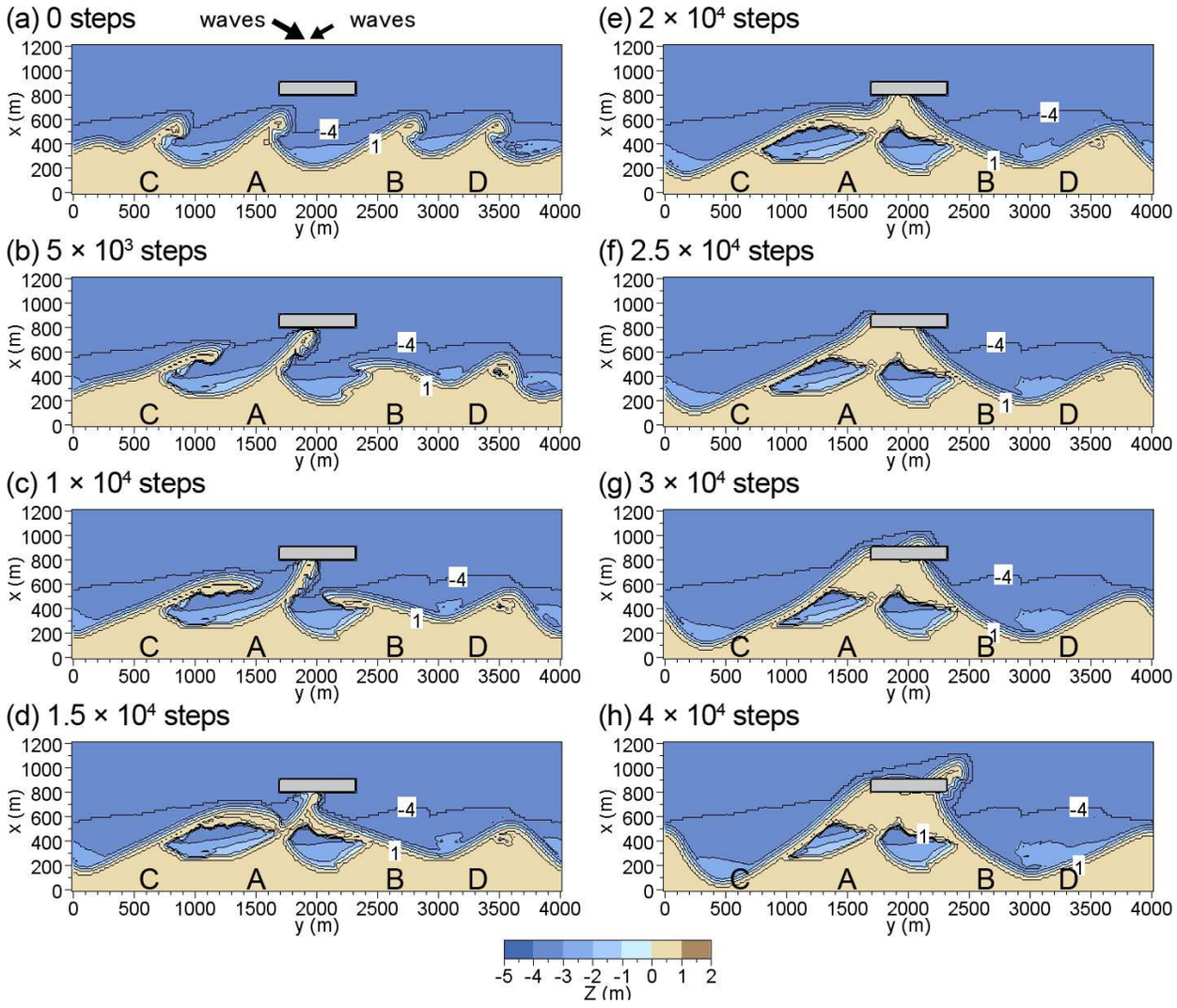

Figure 20. Deformation of sand spits formed under oblique wave incidence from ±60° with probabilities of 0.65:0.35 after construction of breakwater.

Owing to these reasons, the tip of the sand spit A rapidly extended to connect the breakwater until 5×10^3 steps, as shown in Fig. 20(b), and this elongation of the sand spit caused the waves incident from the left to be sheltered in the area right of the breakwater, as shown in Fig. 21(b), resulting in the reversal of the direction of longshore sand transport from rightward to leftward. Thus, the direction of the elongation of sand spit B was reversed and extended toward the lee of the breakwater. Sand spit C also rapidly extended rightward because waves incident from the left were sheltered. The construction of the breakwater further affected the beach changes of sand spit D far from the breakwater, and rightward development ceased and a rounded shoreline was formed.

After 1×10^4 steps, sand spit B rapidly extended to the lee of the breakwater, and after 1.5×10^4 steps, sand spits B and C markedly elongated to connect to sand spit A, leaving two lagoons behind the breakwater. After 2×10^4 steps, sand spit B reduced to a tombolo along with the connection of sand spit C with A. After 2.5×10^4 steps, a double tombolo developed, leaving

two lagoons behind. After 3×10^4 steps, sand was deposited offshore of the breakwater to form a sandy beach, and after 4×10^4 steps, a new sand spit started to extend from the right end of the breakwater because of the net rightward sand transport.

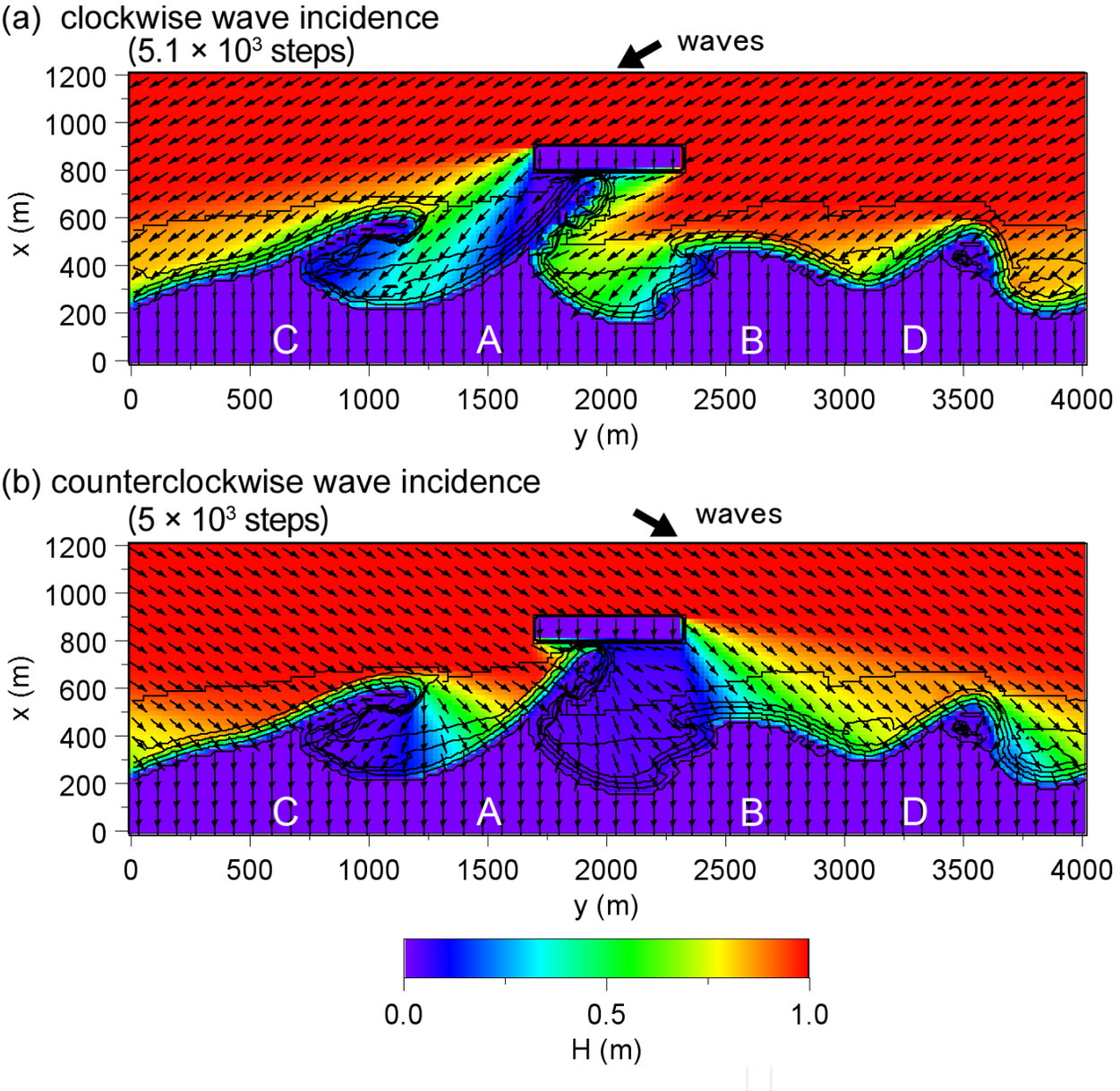

Figure 21. Wave field around a breakwater after 5.1×10^3 and 5×10^3 steps.

4.3. Discussion

The beach changes observed when a breakwater was constructed, as shown in Fig. 19, can be observed in Taman located in southwestern Russia bounded by the Azov Sea and the Black Sea (Fig. 22). Figure 23(a) shows an example of sand bars with two lagoons inside in a shallow water body due to the wave-sheltering effect of a shoal [1]. Sand bars with two lagoons inside have been formed by the wave-sheltering effect by the shoal shown in the lower part of the

http://dx.doi.org/10.5772/57043

figure. The extension of many ridges left of sand bar A shows that waves are incident from the direction normal to shoreline (a). A slender sand bar B also extends with protrusions formed by breaching inside the lagoon on the other side. This indicates that sand bar B was formed by the action of waves incident from the direction normal to shoreline (b). Furthermore, at the tip of sand bar A, a small sand spit C extends rightward. Since the white seabed in Fig. 23(a) is assumed to show a shallow seabed covered with sand, a very shallow seabed extends offshore of sand spit C, and on the right side of sand spit C, the seabed depth suddenly increases, implying that sand spit C developed at the corner of the abruptly changed shoreline. This also agrees with the results given in [9]. The fact that the tip of sand spit C extended rightward shows the wave action from direction (b).

Thus, the sand bars were formed when waves were incident to the coast from two directions in a shallow sea with an offshore shoal. Although the wave-sheltering effect was produced by a shoal in Fig. 23(a), the same results were obtained in this study, when a breakwater was constructed. Figure 23(b) is the same results as shown in Fig. 20(h). The calculation results are in good agreement with the example of the formation of the sand bars with two lagoons inside and the formation of small sand spit C in Fig. 23(a).

In Figs. 14 and 15, which show the results on a coast with predominant longshore sand transport, a sand spit elongated at the tip of the structure owing to the successive sand supply from the upcoast. This elongation of a sand spit well explains the results observed at Santa Barbara in California [22].

Figure 22. Location of study area near Azov Sea.

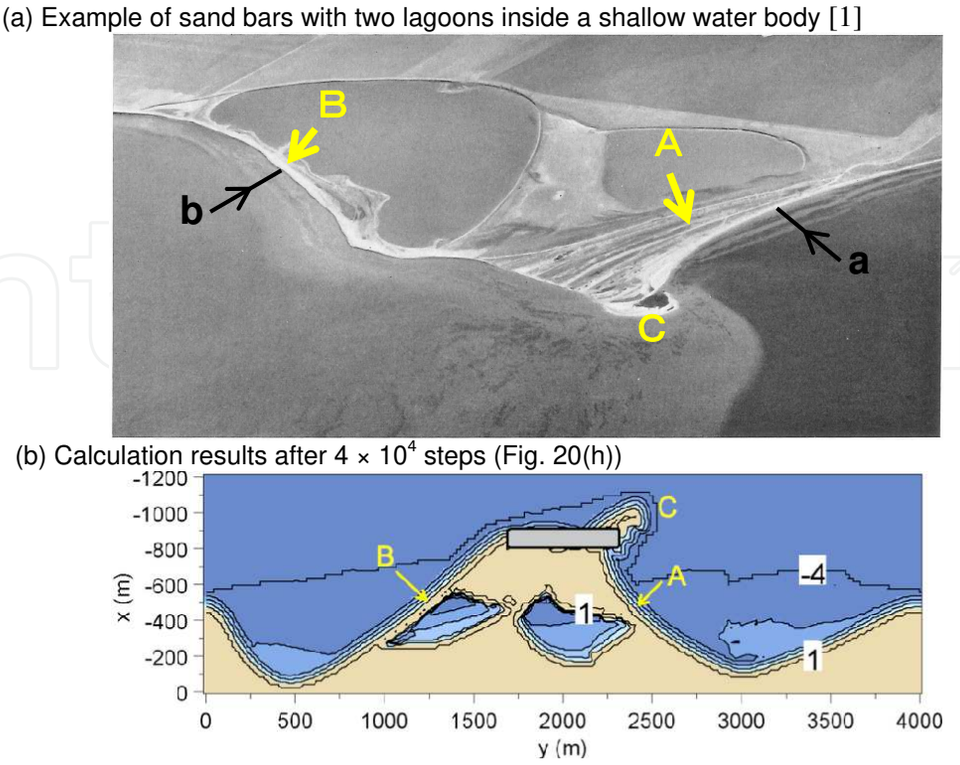

Figure 23. Comparison of measured and calculated double and looped spits.

5. Conclusions

Regarding the development of multiple sand spits and cuspate forelands with rhythmic shapes observed along the shore of the Azov Sea [1], the BG model was used to simulate the shoreline evolution caused by high-angle wave instability. The wave direction was assumed to be obliquely incident from 60°, 50° and 40° counterclockwise or from the directions of ±60° with probabilities of 0.5:0.5 and 0.60:0.40, 0.65:0.35, 0.70:0.30, 0.75:0.25 and 0.80:0.20, while determining the direction from the probability distribution at each step. As a result, the 3-D development of multiple sand spits and cuspate forelands with rhythmic shapes was successfully explained by the present model and the results of the previous study in [2] were reconfirmed and reinforced. Because the wave field was predicted using the energy balance equation for irregular waves in this study, the wave field including wave refraction, wave breaking and the wave-sheltering effect can be systematically predicted. In addition, because 2-D sand transport equations were employed in our model, in contrast to the model in [2] in which the longshore sand transport formula was used, this model has the advantages of the conventional 3-D model for predicting beach changes for various applications.

In addition to the prediction of the development of sand spits and cuspate forelands with rhythmic shapes owing to the high-angle wave instability under natural conditions, the impact of anthropogenic factors, such as the construction of a groin or a breakwater, on the beach

changes was predicted. It was concluded that the construction of a groin had a marked impact on the sandy beach; the alteration from the field with the development of the sand spits to that with the elongation of a single sand spit, as well as the acceleration of offshore sand transport because of the blockage of longshore sand transport.

Author details

Takaaki Uda[1], Masumi Serizawa[2] and Shiho Miyahara[2]

1 Public Works Research Center, Tokyo, Japan

2 Coastal Engineering Laboratory Co., Ltd., Tokyo, Japan

References

[1] Zenkovich, V. P. (1967). Processes of Coastal Development, Interscience Publishers, New York, p. 751.

[2] Ashton, A., Murray, A. B., Arnault, O. (2001). Formation of coastline features by large-scale instabilities induced by high angle waves, Nature, Vol. 414, pp. 296-300.

[3] Ashton, A., Murray, A. B. (2006). High-angle wave instability and emergent shoreline shapes: 1. Modeling of sand waves, flying spits, and capes: Jour. Geophys. Res., Vol. 111, F04011, doi: 10.1029/2005JF000422.

[4] Littlewood, R., Murray, A. B., Ashton, A. D. (2007). An alternative explanation for the shape of 'Log-Spiral' Bays, Coastal Sediments '07, pp. 341-350.

[5] Serizawa, M., Uda, T., Miyahara, S. (2012). Prediction of development of sand spits and cuspate forelands with rhythmic shapes caused by shoreline instability using BG model, Proc. 33rd ICCE, sediment.35, pp. 1-11.

[6] Falqués, A., van den Berg, N., Calvete, D. (2008). The role of cross-shore profile dynamics on shoreline instability due to high-angle waves, Proc. 31st ICCE, pp. 1826-1838.

[7] Inman, D. L., Bagnold, R. A. (1963). Littoral processes, In The Sea, Hill, M. N., Vol. 3, Wiley, New York, pp. 529-533.

[8] Bagnold, R. A. (1963). Mechanics of marine sedimentation, In The Sea, Hill, M. N., Vol. 3, Wiley, New York, pp. 507-528.

[9] Serizawa, M., Uda, T. (2011). Prediction of formation of sand spit on coast with sudden change using improved BG model, Coastal Sediments '11, pp. 1907-1919.

[10] Serizawa, M., Uda, T., Miyahara, S. (2013). Effects of anthropogenic factors on development of sand spits and cuspate forelands with rhythmic shapes, Asian and Pacific Coasts 2013, Proc. 7th International Conf. pp. 9-16.

[11] Ozasa, H., Brampton, A. H. (1980). Model for predicting the shoreline evolution of beaches backed by seawalls, Coastal Eng., Vol. 4, pp. 47-64.

[12] Serizawa, M., Uda, T., San-nami, T., Furuike, K. (2006). Three-dimensional model for predicting beach changes based on Bagnold's concept, Proc. 30th ICCE, pp. 3155-3167.

[13] Mase, H. (2001). Multidirectional random wave transformation model based on energy balance equation, Coastal Eng. J., JSCE, Vol. 43, No. 4, pp. 317-337.

[14] Dally, W. R., Dean, R. G., Dalrymple, R. A. (1984). A model for breaker decay on beaches, Proc. 19th ICCE, pp. 82-97.

[15] Katayama, H., Goda, Y. (2002). Beach changes due to suspended sediment picked up by random breaking waves, Proc. 28th ICCE, pp. 2767-2779.

[16] Serizawa, M., Uda, T., San-nami, T., Furuike, K. (2003). Prediction of depth changes on x-y meshes by expanding contour-line change model, Ann. J. Coastal Eng. JSCE, 50, pp. 476-480. (in Japanese)

[17] Goda, Y. (1985). Random Seas and Design of Maritime Structures. University of Tokyo Press, Tokyo, p. 323.

[18] Uda, T., Yamamoto, K. (1991). Spit formation in lake and bay, Coastal Sediments '91, Vol. 2, pp. 1651-1665.

[19] van den Berg, N., Falqués, A., Ribasz, F. (2011). Long-term evolution of nourished beaches under high angle wave conditions, J. Marine Systems, Vol. 88, Issue. 1, pp. 102-112.

[20] Bird, E. (2000). Coastal Geomorphology: An Introduction, Wiley, England, p. 322.

[21] Davis, R. A., FitzGerald, D. M. (2004). Beaches and Coasts, Blackwell, Malden, p. 419.

[22] Komar, P. D. (1998). Beach Processes and Sedimentation, Prentice Hall, New Jersey, 2nd ed., p. 544.